# A novel isoform of myosin 18A (Myo18A$\gamma$) is an essential sarcomeric protein in mouse heart

Received for publication, June 21, 2018, and in revised form, January 19, 2019 Published, Papers in Press, February 8, 2019, DOI 10.1074/jbc.RA118.004560

**Markus Horsthemke[a], Lauryl M. J. Nutter[b], Anne C. Bachg[a], Boris V. Skryabin[c], Ulrike Honnert[a], Thomas Zobel[d], Sven Bogdan[e], Monika Stoll[f], Matthias D. Seidl[g], Frank U. Müller[g], Ursula Ravens[h], Andreas Unger[i], Wolfgang A. Linke[i], Pim R. R. van Gorp[j], Antoine A. F. de Vries[j], Martin Bähler[a], and Peter J. Hanley[a1]**

*From the [a]Institut für Molekulare Zellbiologie, [c]Department of Medicine, Transgenic Animal and Genetic Engineering Models (TRAM), [f]Institut für Humangenetik, and [g]Institut für Pharmakologie und Toxikologie, Westfälische Wilhelms-Universität Münster, 48149 Münster, Germany, the [b]Centre for Phenogenomics, Hospital for Sick Children, Toronto, Ontario M5T 3H7, Canada, the [d]Center for Advanced Imaging, Heinrich Heine Universität Düsseldorf, 40225 Düsseldorf, Germany, the [e]Institut für Physiologie und Pathophysiologie, Abteilung Molekulare Zellphysiologie, Philipps-Universität Marburg, 35037 Marburg, Germany, the [h]Institut für Experimentelle Kardiovaskuläre Medizin, Universitätsklinikum Freiburg, 79110 Freiburg, Germany, the [i]Institut für Physiologie II, Westfälische Wilhelms-Universität Münster, Robert-Koch-Strasse 27b, 48149 Münster, Germany, and the [j]Laboratory of Experimental Cardiology, Department of Cardiology, Leiden University Medical Center, Albinusdreef 2, 2300 RC Leiden, The Netherlands*

Edited by Velia M. Fowler

**Whereas myosin 18B (Myo18B) is known to be a critical sarcomeric protein, the function of myosin 18A (Myo18A) is unclear, although it has been implicated in cell motility and Golgi shape. Here, we show that homozygous deletion (homozygous tm1a, tm1b, or tm1d alleles) of *Myo18a* in mouse is embryonic lethal. Reminiscent of *Myo18b*, *Myo18a* was highly expressed in the embryo heart, and cardiac-restricted *Myo18a* deletion in mice was embryonic lethal. Surprisingly, using Western blot analysis, we were unable to detect the known isoforms of Myo18A, Myo18A$\alpha$ and Myo18A$\beta$, in mouse heart using a custom C-terminal antibody. However, alternative anti-Myo18A antibodies detected a larger than expected protein, and RNA-Seq analysis indicated that a novel Myo18A transcript is expressed in mouse ventricular myocytes (and human heart). Cloning and sequencing revealed that this cardiac isoform, denoted Myo18A$\gamma$, lacks the PDZ-containing N terminus of Myo18A$\alpha$ but includes an alternative N-terminal extension and a long serine-rich C terminus. EGFP-tagged Myo18A$\gamma$ expressed in ventricular myocytes localized to the level of A-bands in sarcomeres, and *Myo18a* knockout embryos at day 10.5 exhibited disorganized sarcomeres with wavy thick filaments. We additionally generated myeloid-restricted *Myo18a* knockout mice to investigate the role of Myo18A in nonmuscle cells, exemplified by macrophages, which express more Myo18A$\beta$ than Myo18A$\alpha$, but no defects in cell shape, motility, or Golgi shape were detected. In summary, we have identified a previously unrecognized sarcomere component, a large novel isoform (denoted Myo18A$\gamma$) of Myo18A. Thus, both members of class XVIII myosins are critical components of cardiac sarcomeres.**

Myosins are a superfamily of motor proteins, encoded in mice by 39 genes, which have been categorized into 12 classes (I, II (conventional myosins), III, V, VI, VII, IX, X, XV, XVI, XVIII, and XIX) (1, 2). Class XVIII myosins consist of Myo18A and Myo18B. The longest known splice variant of Myo18A (denoted Myo18A$\alpha$), initially termed MysPDZ (myosin containing PDZ domain) (3), has a distinctive N-terminal extension, which includes a highly charged KE (lysine-glutamine)-rich region and a PDZ domain (3–5). In contrast, a shorter splice variant of Myo18A (denoted Myo18A$\beta$) lacks the N-terminal extension (4, 5). Like Myo18A$\alpha$, Myo18B (as distinct from Myo18A$\beta$) has a long N-terminal extension but lacks a PDZ domain (6). Myo18B was shown to localize to the Z-discs of striated muscle, and *Myo18b* deficiency causes embryonic lethality associated with disordered sarcomeres (7). In contrast, Berger *et al.* (8) found that Myo18B-GFP localizes to sarcomeric A-bands, rather than Z-discs, in zebrafish skeletal muscle, and gene deletion impaired sarcomere assembly. Thus, Myo18B is thought to be important for the development and/or maintenance of sarcomeres.

The physiological function of Myo18A, which is widely expressed (3), is not clear. In 2003, Mori *et al.* (4) inferred that MysPDZ$\alpha$-YFP[2] (Myo18A$\alpha$-YFP) localizes to the Golgi apparatus, and, subsequently, Dippold *et al.* (9) observed that knockdown of *Myo18a* using siRNA induces aberrant compacted Golgi, which is rescued by concomitant Myo18A-GFP expression. The rescue failed when the putative ATPase pocket was mutated, suggesting that Myo18A motor activity is responsible for the elongated morphology of Golgi. However, in an elaborate study, Bruun *et al.* (10) could not find a link between Myo18A and Golgi morphology. Moreover, data obtained

This work was supported by Deutsche Forschungsgemeinschaft (DFG) Grants Mu1376/11-3 (to F. U. M.), HA 3271/3-1 (to P. J. H.), HA 3271/4-1 (to P. J. H.), and EXC 1003 (Cluster of Excellence 1003), Cells in Motion (CiM), and the NorCOMM2 project was funded by Genome Canada and Ontario Genomics Institute Grant OGI-059. The authors declare that they have no conflicts of interest with the contents of this article.
This article was selected as one of our Editors' Picks.
This article contains Figs. S1–S6.
[1] To whom correspondence should be addressed. E-mail: hanley@uni-muenster.de.

[2] The abbreviations used are: YFP, yellow fluorescent protein; EYFP, enhanced yellow fluorescent protein; HET, heterozygous; KOMP, Knockout Mouse Project; *E*, embryonic day; cKO, conditional knockout; X-gal, 5-bromo-4-chloro-3-indolyl $\beta$-D-galactoside; EGFP, enhanced green fluorescent protein; NRVM, neonatal rat ventricular myocyte; *IRES*, internal ribosome entry site; NBCS, newborn calf serum; FCS, fetal calf serum; SR-SIM, superresolution structured illumination microscopy.

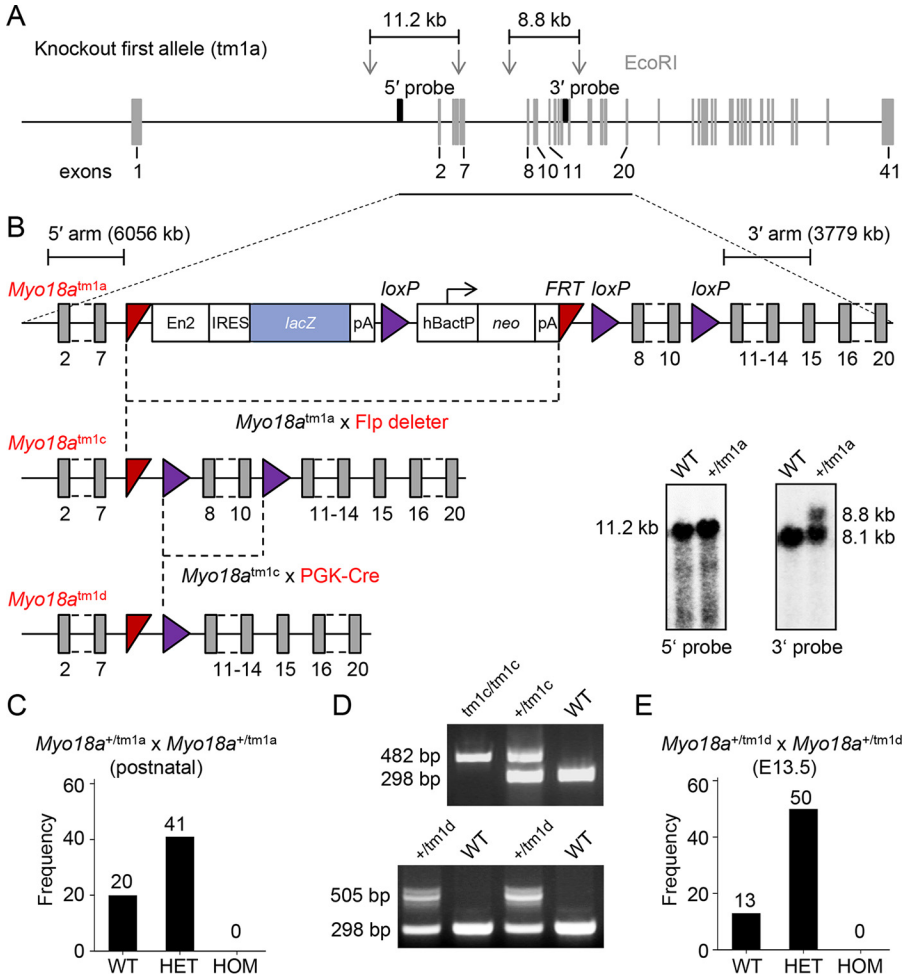


**Figure 1. Homozygous *Myo18a* deletion is lethal.** *A* and *B*, schematic diagram of the *Myo18a* knockout first targeting strategy and conversion of the tm1a (knockout first) allele to tm1c (floxed) and tm1d (knockout) alleles, respectively. Germ line deletion of *Myo18a* was produced by interbreeding *Myo18a*$^{tm1c}$ and PGK-Cre mice (to yield *Myo18a*$^{tm1d}$). *Myo18a* targeting was confirmed by Southern blot analysis. *C*, PCR genotyping of offspring derived from crossing HET knockout first (*Myo18a*$^{+/tm1a}$ × *Myo18a*$^{+/tm1a}$) mice. Notably, no mice HOM for the knockout first allele were detected. *D*, PCR genotyping of offspring derived from crossing heterozygous floxed (*Myo18a*$^{+/tm1c}$ × *Myo18a*$^{+/tm1c}$) or heterozygous *Myo18a* knockout (*Myo18a*$^{+/tm1d}$ × *Myo18a*$^{+/tm1d}$) mice. *E*, no homozygous *Myo18a* knockout (*Myo18a*$^{tm1d/tm1d}$) mice were detected at E13.5, indicating that *Myo18a* deletion is embryonic lethal.

with recombinant proteins indicate that *Drosophila* Myo18 (CG31045) and mouse Myo18A do not exhibit motor activity but, instead, probably act as tether molecules (11, 12). In accord, Taft *et al.* (13) found that the motor domain of human Myo18A lacks intrinsic or actin-activated ATPase activity. In addition to its putative role in shaping the Golgi, Myo18A has been implicated in modulating membrane protrusive activity and cell migration (14), whereas Yang *et al.* (15) identified Myo18A as a receptor for surfactant protein A.

Interestingly, Mori *et al.* (4) reported that Myo18A$\beta$ is expressed in immature macrophage-like cells, whereas Myo18A$\alpha$ expression first emerges in mature cells, suggesting that Myo18A may have a special role in macrophage function. The authors also found in subsequent work that Myo18A$\alpha$ (or the N-terminal extension alone), but not Myo18A$\beta$, localized to actin filaments and the plasma membrane (5). In contrast, Billington *et al.* (16) recently reported that both Myo18A$\alpha$ and Myo18A$\beta$ can coassemble with NMHC-IIA (nonmuscle myosin (heavy chain) IIA) to form mixed bipolar filaments. Here, we used various *Myo18a* knockout mouse models, including reporter knockout and conditional knockout models, to elucidate the physiological function of Myo18A.

## Results

### *Myo18a deletion in mice is embryonic lethal*

We started out with heterozygous (HET) *Myo18a* knockout first (denoted *Myo18a*$^{+/tm1a}$) mice, obtained from the Knockout Mouse Project (KOMP), the targeting strategy of which is delineated in Fig. 1 (*A* and *B*). Notably, these mice harbor a gene expression reporter (*lacZ*) and have conditional knockout potential (Fig. 1*B*). Southern blot analysis confirmed correct targeting of the *Myo18a* gene (Fig. 1*B*). Interbreeding heterozygous knockout first (*Myo18a*$^{+/tm1a}$) mice failed to produce homozygous (HOM) *Myo18a* knockout first mice (Fig. 1*C*), implying that targeted disruption of *Myo18a* function is lethal. Subsequently, *Myo18a* knockout first mice were crossed with Flp deleter mice, which ubiquitously express Flp recombinase, thereby allowing deletion of the FRT flanked sequence (*lacZ* reporter and selection cassettes) (see Fig. 1*B*). Importantly, in support of correct targeting, the WT PCR product (298 bp)

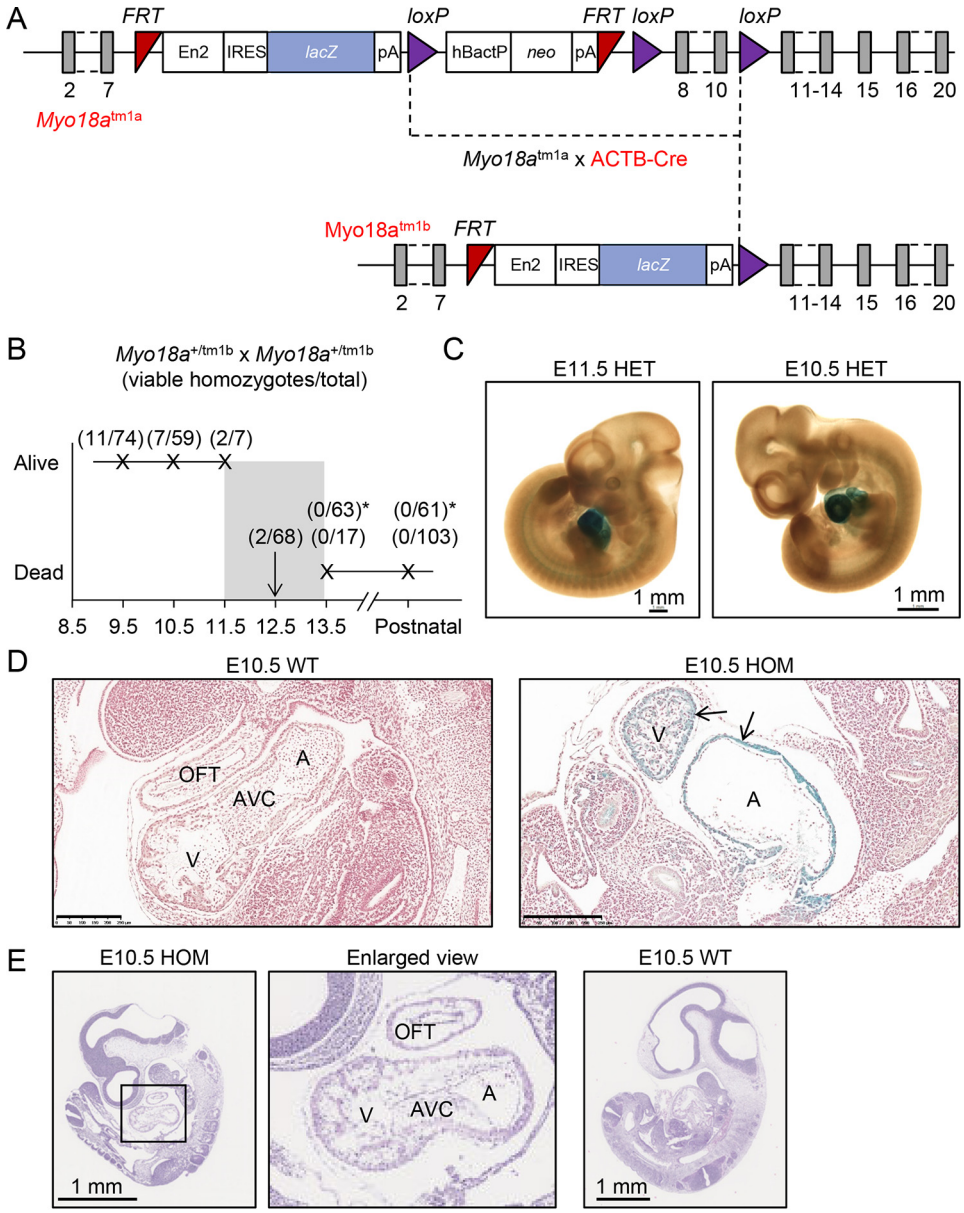


**Figure 2. X-gal staining and histology of *Myo18a*$^{tm1b}$ embryos.** *A*, conversion of the tm1a (knockout first) allele to the tm1b (reporter knockout) allele by crossing heterozygous knockout first (*Myo18a*$^{+/tm1a}$) mice with ACTB-Cre mice. *B*, timing of embryonic lethality by timed intercrossings of heterozygous knockout reporter (*Myo18a*$^{+/tm1b}$) mice. No viable homozygous embryos were detected after E12.5. *, data from crossing *Myo18a*$^{+/tm1a}$ × *Myo18a*$^{+/tm1a}$. *C*, whole-mount X-gal staining of HET *Myo18a* reporter knockout embryos at E11.5 and E10.5. *Scale bars*, 1 mm. *D*, histological sections of the heart obtained from X-gal–stained WT and HOM *Myo18a* reporter knockout E10.5 embryos. *Arrows*, X-gal staining of myocardial cells. *Scale bars*, 250 μm. *AVC*, atrioventricular cushions; *V*, ventricle; *A*, atrium. *E*, hematoxylin and eosin (*HE*) staining of sagittal sections of E10.5 HOM knockout (*Myo18a*$^{tm1b/tm1b}$) and WT embryos. *OFT*, outflow tract; *AVC*, atrioventricular cushions; *V*, ventricle; *A*, atrium.

disappeared in homozygous floxed *Myo18a* (*Myo18a*$^{tm1c/tm1c}$) mice (Fig. 1*D*). Floxed mice were crossed with PGK-Cre mice (see Fig. 1*B*), which maternally express Cre recombinase, to delete the *loxP* flanked exons 8, 9, and 10 and generate global cassette-free heterozygous *Myo18a* knockout mice (*Myo18a*$^{+/tm1d}$; Fig. 1*D*). Intercrossing heterozygous *Myo18a* knockout (*Myo18a*$^{+/tm1d}$) mice failed to produce homozygous *Myo18a* knockout (*Myo18a*$^{tm1d/tm1d}$) mice postnatally or at embryonic day 13.5 (E13.5) (Fig. 1*E*). Thus, disruption of *Myo18a* is clearly embryonic lethal.

The timing of embryonic lethality was further investigated using timed matings of heterozygous knockout reporter (*Myo18a*$^{+/tm1b}$) mice, produced by intercrossing *Myo18a* knockout first (*Myo18a*$^{+/tm1a}$) mice with a Cre deleter strain (ACTB-Cre; Fig. 2*A*). The *Myo18a*$^{+/tm1b}$ × *Myo18a*$^{+/tm1b}$ crossings produced embryos with a *lacZ* gene expression reporter. Viable *Myo18a*$^{tm1b/tm1b}$ embryos could be detected at E9.5, E10.5, and E11.5, whereas only 2 of the 12 homozygous knockout embryos detected at E12.5 were alive. No *Myo18a*$^{tm1b/tm1b}$ (or Myo18a$^{tm1d/tm1d}$; see Fig. 1*E*) embryos were recovered at E13.5 (Fig. 2*B*).

Whole-mount X-gal staining of heterozygous (*Myo18a*$^{+/tm1b}$) embryos at E11.5 and E10.5 (Fig. 2*C*) revealed predominant expression of *Myo18a* in the heart. Histological sections of X-gal–stained embryos showed *Myo18a* expression in developing atrial and ventricular myocytes (Fig. 2*D*). Heart chamber

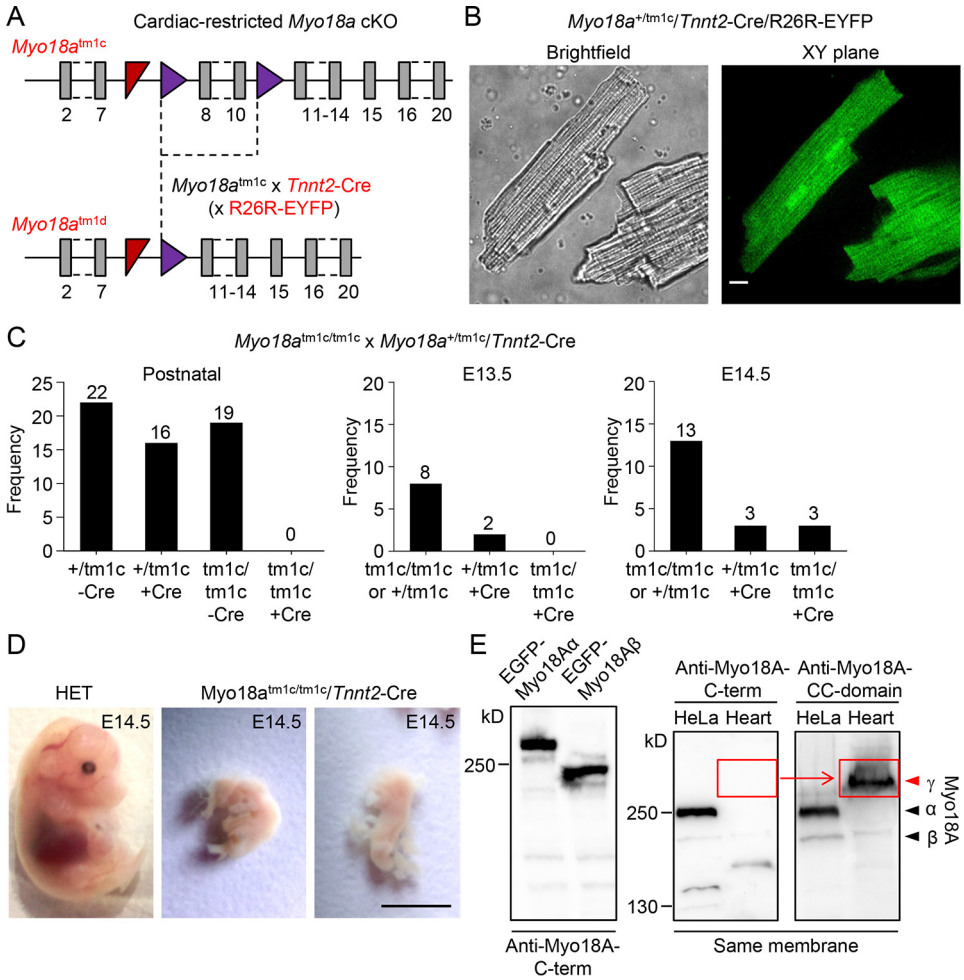


**Figure 3. Mouse ventricular myocytes express a novel isoform of Myo18A and cardiac-restricted *Myo18a* deletion is lethal.** *A*, generation of cardiac-restricted *Myo18a* knockout mice. Mice harboring the floxed *Myo18a* allele (*Myo18a*$^{tm1c}$) were crossed with *Tnnt2*-Cre mice, in which Cre recombinase is expressed in cardiac myocytes. Conditional knockout mice were further crossed with Cre reporter (R26R-EYFP) mice to derive triple mutant (cardiac-restricted *Myo18a* knockout with Cre reporter) mice. *B*, bright field and fluorescence images of ventricular myocytes isolated from a *Myo18a*$^{+/tm1c}$/*Tnnt2*-Cre/R26R-EYFP mouse. *Green* (EYFP) fluorescence is an indicator of Cre recombinase activity. *Scale bar*, 10 $\mu$m. *C*, no homozygous cardiac-restricted *Myo18a* knockout (*Myo18a*$^{tm1c/tm1c}$/*Tnnt2*-Cre) mice were obtained after crossing *Myo18a*$^{tm1c/tm1c}$ and Myo18a$^{+/tm1c}$/*Tnnt2*-Cre mice, indicating that conditional deletion of *Myo18a* in cardiac myocytes is lethal. No *Myo18a*$^{tm1c/tm1c}$/*Tnnt2*-Cre embryos were detected at E13.5, and three dead embryos were detected at E14.5. *D*, photographs of HET and homozygous cardiac-restricted *Myo18a* knockout embryos at day E14.5. *Scale bar*, 0.5 mm. *E*, Western blotting analyses. A custom antibody against the last 18 amino acids of mouse Myo18A (anti-Myo18A-C-term) recognizes the Myo18A isoforms Myo18A$\alpha$ and Myo18A$\beta$. Lysates were prepared from HeLa cells transiently expressing EGFP-Myo18A$\alpha$ (mouse) or EGFP-Myo18A$\beta$ (mouse). The custom anti-Myo18A-C-term antibody did not detect Myo18A in mouse heart lysate, whereas an antibody against the coiled-coil (*CC*) domain of Myo18A detected a larger than expected band on the same membrane.

formation, which follows heart tube lengthening and looping at around E8.5 (17), could be observed in E10.5 *Myo18a*$^{tm1b/tm1b}$ embryos (Fig. 2*E*).

### *Generation of cardiac-restricted Myo18a knockout mice and identification of a novel Myo18A isoform in the heart*

The high expression of *Myo18a* in the heart and embryonic lethality around E12.5 in homozygous *Myo18a* knockout mice suggested that Myo18A may be critical for cardiac development and/or function. However, a recent study highlighted that placental defects in mouse gene knockouts may be major contributors to early embryonic lethality (E9.5–E14.5) (18). To determine the importance of Myo18A in the heart, we generated cardiomyocyte-restricted *Myo18a* knockout mice by crossing floxed *Myo18a* mice (tm1c allele) with *Tnnt2*-Cre mice (Fig. 3*A*), which confer Cre recombination restricted to the heart starting at E7.5 (19). We further crossed the offspring with R26R-EYFP (B6.129X1-*Gt(ROSA)26Sor*$^{tm1(EYFP)Cos}$/J) mice so that individual Cre-positive myocytes could be identified by the expression of enhanced yellow fluorescent protein (EYFP). All living ventricular myocytes isolated from triple mutant (*Myo18a*$^{+/tm1c}$/*Tnnt2*-Cre/R26R-EYFP) mice and imaged by spinning disk confocal microscopy were EYFP-positive (Fig. 3*B*). Intercrossing of homozygous floxed (*Myo18a*$^{tm1c/tm1c}$) and *Myo18a*$^{+/tm1c}$/*Tnnt2*-Cre mice failed to generate *Myo18a*$^{tm1c/tm1c}$/*Tnnt2*-Cre offspring (Fig. 3*C*), implying that cardiac-restricted *Myo18a* deletion is lethal. Moreover, using timed pregnancies, we could only detect the remnants of *Myo18a*$^{tm1c/tm1c}$/*Tnnt2*-Cre embryos at E14.5 (Fig. 3, *C* and *D*).

Next, we investigated which isoforms of Myo18A are expressed in the heart. We generated an affinity-purified rabbit antibody against the last 18 amino acids of mouse Myo18A

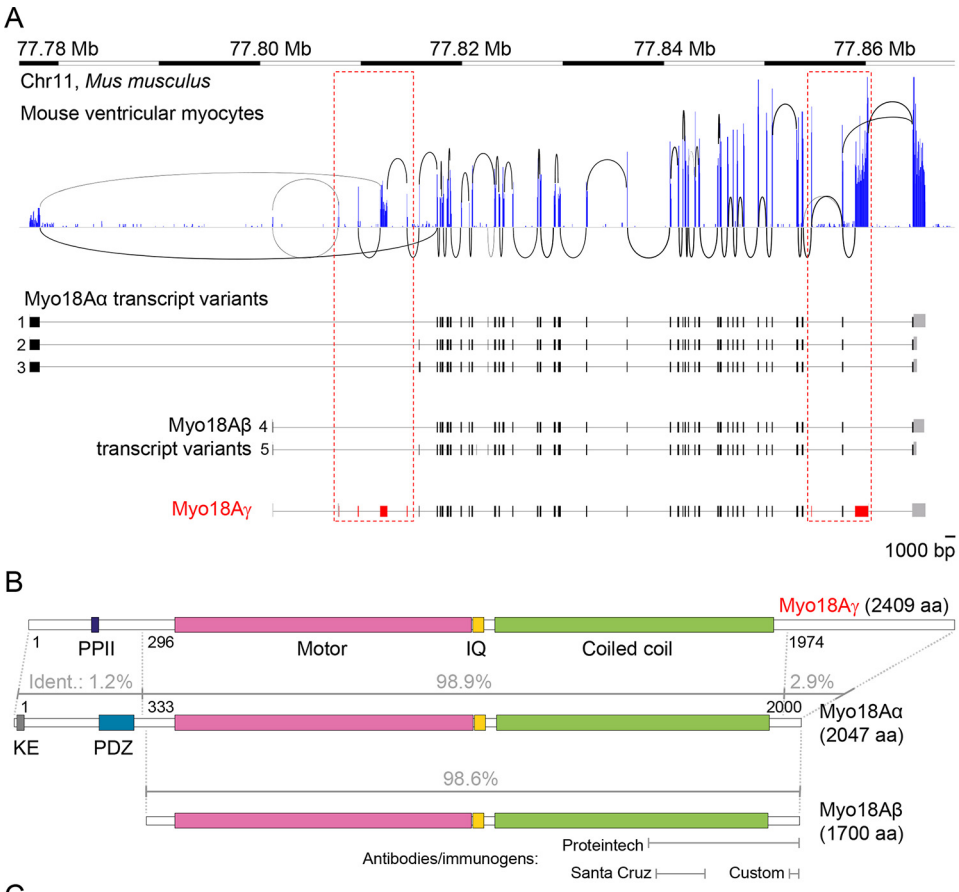


**Figure 4. Cloning and sequencing of the novel isoform of Myo18A expressed in mouse ventricular myocytes.** *A*, representative Sashimi plot of data obtained by mouse ventricular myocyte RNA-Seq ($n = 6$ mice). Exons are *colored blue*, and splice junction reads are depicted as *arcs*. The *red rectangles* (with *dashed lines*) indicate exons that are abundant in the ventricular myocyte transcript but absent in the aligned annotated genomic references corresponding to transcripts for Myo18A$\alpha$ and Myo18A$\beta$. *B*, domain structure of the novel cardiac isoform of Myo18A, Myo18A$\gamma$, as well as, for comparison, the domain structures of Myo18A$\alpha$ and Myo18A$\beta$. The recognition sites of various anti-Myo18A antibodies used in this study are indicated *below*. Notably, the custom (anti-Myo18A-C-term) antibody is unable to recognize the novel C terminus of Myo18A$\gamma$. *PPII*, polyproline II helix; *KE*, KE-rich region; *PDZ*, PDZ domain; *IQ*, IQ motif. *C*, alignment of the N-terminal protein sequence of Myo18A$\gamma$, derived from cloning and sequencing cDNA from mouse ventricular myocytes, with a mouse protein sequence of 219 residues from the Ensembl database (MGP_FVBNJ_P0030691).

(anti-Myo18A-C-term) and confirmed using Western blotting (Fig. 3*E*) that it recognizes EGFP-tagged mouse Myo18A$\alpha$ and mouse Myo18A$\beta$, overexpressed in HeLa cells (Fig. 3*E*). Nevertheless, we were unable to detect either Myo18A$\alpha$ or Myo18A$\beta$ in lysates from adult mouse heart (Fig. 3*E*). Similarly, Yang *et al.* (15) were unable to detect Myo18A in either heart or skeletal muscle using anti-Myo18A-C-term antibodies. However, using the same membrane, we were able to identify a larger than expected band (see *red arrows* in Fig. 3*E*) with alternative anti-Myo18A coiled-coil domain (*Anti-Myo18A-CC-domain*) antibodies from Proteintech (Fig. 3*E*) and Santa Cruz (not shown). We suspected that a large novel isoform of Myo18A with an alternative C terminus is expressed in the heart. To investigate alternative exon expression in the heart, we isolated RNA from mouse ventricular myocytes and performed next-generation sequencing (Fig. 4*A*). Quantitative visualization of the raw data (splicing events) from a single mouse heart in the form of a Sashimi plot (20), aligned to reference genome sequences, revealed that mouse ventricular myocytes express two large exons (highlighted by *red rectangles* in Fig. 4*A*), as well as sev-

eral additional smaller exons, which are not found in the transcripts for Myo18Aα or Myo18Aβ. We cloned and sequenced the cardiac transcript, after performing 5′- and 3′-RACE (rapid amplification of cDNA ends) PCR and long-range PCRs, which confirmed that the cardiac Myo18A isoform, denoted Myo18Aγ (GenBank™ accession number MK268687), has novel N and C termini (see Myo18Aγ domain structure shown in Fig. 4*B*). This explains why our custom antibody directed against the last 18 amino acids of Myo18Aα (and Myo18Aβ), as indicated in Fig. 4*B*, was unable to detect the cardiac isoform of Myo18A, Myo18Aγ. Notably, the unique N-terminal extension (containing KE-rich and PDZ domains) encoded by exon 1 of *Myo18aα* is absent in Myo18Aγ. Instead, Myo18Aγ has an alternative N-terminal extension (Fig. S1), containing a polyproline region, and a long alternative C terminus (Fig. S2), relative to Myo18Aα (Fig. 4*B*), which is rich in serine residues (Fig. S2). Notably, the deduced N-terminal protein sequence of Myo18Aγ, including the start, nicely matches a mouse protein sequence from the Ensembl database (Fig. 4*C*). Myo18Aγ has a predicted molecular mass of 267 kDa, considerably larger than Myo18Aα (230 kDa) and Myo18Aβ (190 kDa).

### *Human homolog of mouse Myo18Aγ*

RNA sequence analysis of human atrial tissue revealed additional exons that are not found in reference human MYO18A transcripts (Fig. 5*A*). Sequence alignment confirmed that these exons code a protein homolog of mouse Myo18Aγ (Fig. 5*B*). Multiple sequence alignment generated by the program Clustal Omega (21, 22), using predicted translated transcripts (denoted by the accession prefix XM_) identified by tblastn (protein to translated nucleotide BLAST (basic local alignment search tool)) as input, indicated that the N and C termini of mouse Myo18Aγ are well-conserved across mammalian species (Figs. S3 and S4), except no significant similarity to the C terminus was found in rabbit (*Oryctolagus cuniculus*). Comparison of mouse Myo18Aγ with the predicted sequences in nonmammalian species revealed high identity in the last 18 residues of the N terminus (Fig. S5) and high identity in scattered regions in the C terminus (Fig. S6). No significant similarity to the N and C termini of mouse Myo18Aγ was found in *Drosophila melanogaster* or *Caenorhabditis elegans*.

### *Myo18Aγ-EGFP localizes to the A-band of cardiac sarcomeres*

To elucidate the subcellular localization of Myo18Aγ, we transfected neonatal rat ventricular myocytes (NRVMs) with EGFP-tagged Myo18Aγ (Fig. 6). Myo18Aγ-EGFP localized between Z-lines in NRVMs stained with antibodies against α-actinin, a Z-disc marker (*first column* in Fig. 6, *A* and *B*). Similarly, in NRVMs cotransfected with the Z-disc marker mScarlet-I-Cypher Ic, Myo18Aγ-EGFP localized between Z-discs (*middle column* in Fig. 6, *A* and *B*), indicating an A-band pattern of distribution. The striated pattern of Myo18Aγ-EGFP overlaid with the A-band marker Myl2-mScarlet-I (myosin light chain 2 tagged to mScarlet) (*third column* in Fig. 6, *A* and *B*), which gives a duplet fluorescence pattern in the A-bands due to dark H-zones (see *inset*), indicating that Myo18Aγ-EGFP localizes to the level of A-bands. However, Myo18Aγ-EGFP poorly colocalized with Myl2-mScarlet-I, suggesting that Myo18Aγ may flank the myofibrils at the level of the A-band (*third column* in Fig. 6, *A* and *B*).

### *Ultrastructural analysis of Myo18a-deficient E10.5 embryo hearts*

Transmission EM of E10.5 embryonic hearts from homozygous *Myo18a* knockout ($Myo18a^{tm1b/tm1b}$) mice revealed, compared with age-matched WT controls, overt disorganization of developing myofibrils, sarcomeric disarray, and disruptions of the A-bands (Fig. 7). WT cardiac embryonic myocytes were rich in developing sarcomeres with well-organized structure, including the presence of Z-discs (*Z*), I-bands (*I*), and A-bands (*A*) (Fig. 7*A*). The myofilaments recognizable in the A-bands were dense and oriented in parallel (see *inset* in Fig. 7*A*). In HET *Myo18a* knockout ($Myo18a^{+/tm1b}$) cardiomyocytes, no differences from WT embryonic myofibrils were observed (Fig. 7, *A* and *B*). In contrast, in HOM *Myo18a* knockout ($Myo18a^{tm1b/tm1b}$) myocytes, embryonic myofibrils were only rarely detected. Instead, thick myosin filaments together with I-Z-I brushes were widespread, and a few short sarcomeric formations with loosely packed A-band formations could be detected (Fig. 7*C*).

### *Expression of unconventional myosins in ventricular myocytes*

Interestingly, analysis of the transcriptome of mouse ventricular myocytes indicated that class XVIII myosins (*Myo18a* and *Myo18b*) are the most highly expressed unconventional myosins (Fig. 8*A*). Moreover, the expression levels of class XVIII myosins were higher than those for class II (conventional) myosins (Fig. 8*B*), except for the extraordinarily high expression level of *Myh6*, which encodes the predominant myosin heavy chain of the thick filaments of cardiac sarcomeres in postnatal mice. Myo18B has been reported to be expressed in skeletal muscle, in addition to cardiac muscle (7). Using lysates from mouse skeletal (gastrocnemius) muscle, we could detect a protein band at the same level as cardiac Myo18Aγ (Fig. 8*C*).

### *Generation of myeloid-restricted Myo18a knockout mice and phenotype screen of Myo18a-deficient macrophages*

Immune cells have been reported to predominantly express Myo18Aβ, which lacks the PDZ-containing N-terminal extension (4, 15). However, Myo18Aα becomes detectable in mature macrophages, suggesting that Myo18A may be important in macrophage function (4). To explore the roles of Myo18A in mouse resident macrophages, triple mutant mice with conditional knockout (cKO) of *Myo18a* in myeloid cells and concomitant expression of a fluorescent Cre reporter gene were generated (Fig. 9). First, floxed *Myo18a* mice were crossed with LysM-Cre mice, in which Cre is expressed under the control of the myeloid-restricted M lysozyme gene (23). Second, the offspring were further crossed with R26R-EYFP mice so that individual conditional knockout macrophages could be identified (Fig. 9*A*). EYFP-positive cells were purified from triple mutant ($Myo18a^{tm1c/tm1c}$/LysM-Cre/R26R-EYFP) mice by cell sorting, and Western blot analysis confirmed that Myo18A protein was deleted in $EYFP^+$ cells (Fig. 9*B*). We found that mature (resident peritoneal) macrophages predominantly express

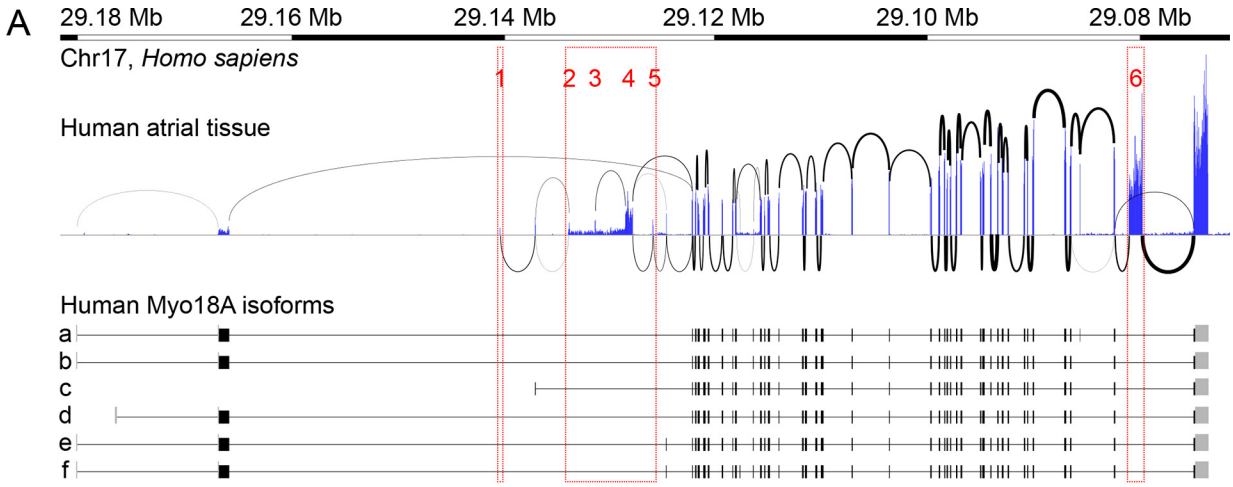
A
29.18 Mb
29.16 Mb
29.14 Mb
29.12 Mb
29.10 Mb
29.08 Mb
Chr17, Homo sapiens
Human atrial tissue
1
2 3 4 5
6
Human Myo18A isoforms
a
b
c
d
e
f

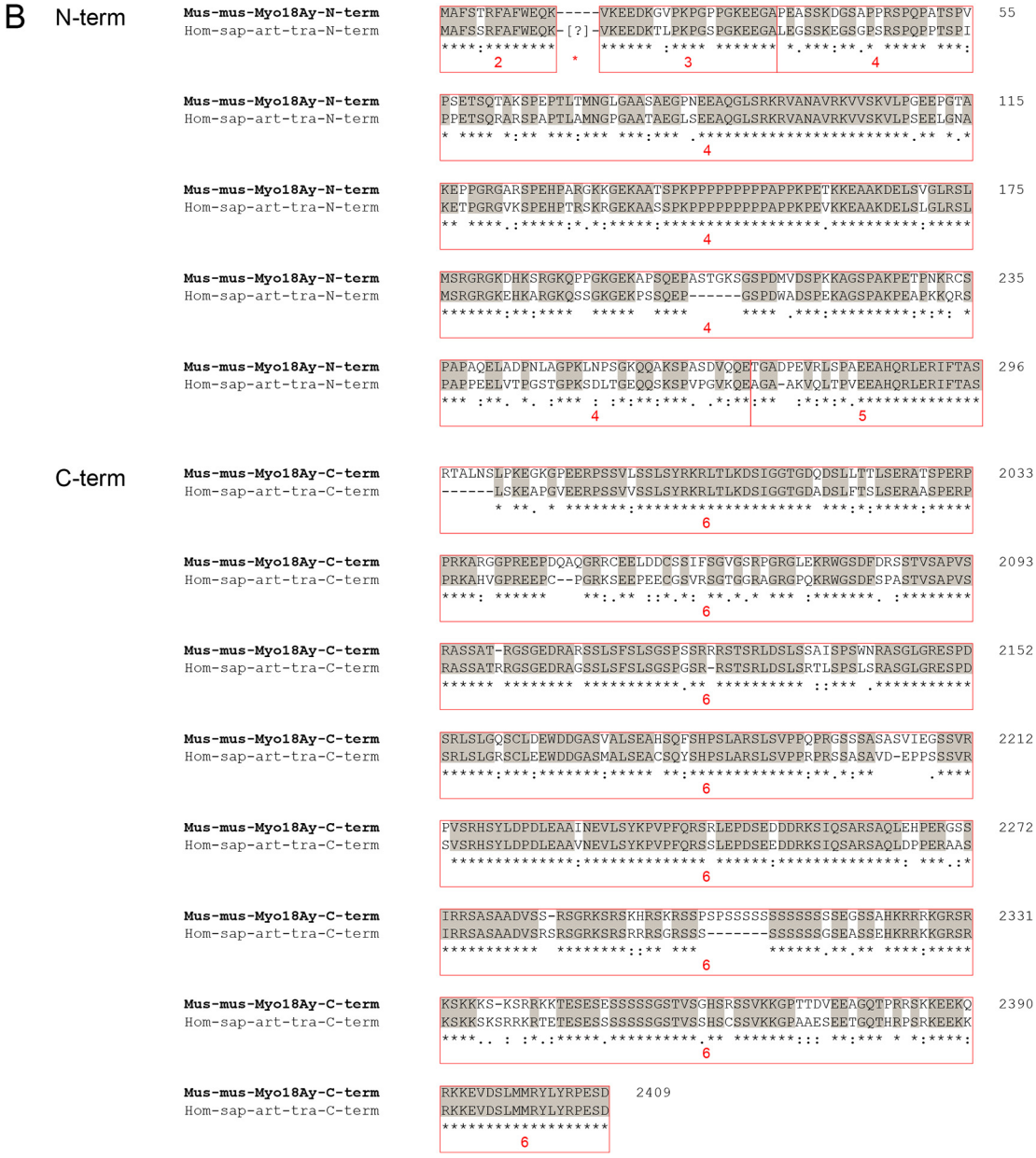
B
N-term
Mus-mus-Myo18Ay-N-term
Hom-sap-art-tra-N-term
MAFSTRFAFWEQK-----VKEEDKGVPKPGPPGKEEGAPEASSKDGSAPPRSPQPATSPV
MAFSSRFAFWEQK-[?]-VKEEDKTLPKPGSPGKEEGALEGSSKEGSGPSRSPQPPTSPI
55
PSETSQTAKSPEPTLTMNGLGAASAEGPNEEAQGLSRKRVANAVRKVVSKVLPGEEPGTA
PPETSQRARSPAPTLAMNGPGAATAEGLSEEAQGLSRKRVANAVRKVVSKVLPSEELGNA
115
KEPPGRGARSPEHPARGKKGEKAATSPKPPPPPPPPAPPKPETKKEAAKDELSVGLRSL
KETPGRGVKSPEHPTRSKRGEKAASSPKPPPPPPPPAPPKPEVKKEAAKDELSLGLRSL
175
MSRGRGKDHKSRGKQPPGKGEKAPSQEPASTGKSGSPDMVDSPKKAGSPAKPETPNKRCS
MSRGRGKEHKARGKQSSGKGEKPSSQEP------GSPDWADSPEKAGSPAKPEAPKKQRS
235
PAPAQELADPNLAGPKLNPSGKQQAKSPASDVQQETGADPEVRLSPAEEAHQRLERIFTAS
PAPPEELVTPGSTGPKSDLTGEQQSKSPVPGVKQEAGA-AKVQLTPVEEAHQRLERIFTAS
296
C-term
Mus-mus-Myo18Ay-C-term
Hom-sap-art-tra-C-term
RTALNSLPKEGKGPEERPSSVLSSLSYRKRLTLKDSIGGTGDQDSLLTTLSERATSPERP
------LSKEAPGVEERPSSVVSSLSYRKRLTLKDSIGGTGDADSLFTSLSERAASPERP
2033
PRKARGGPREEPDQAQGRRCEELDDCSSIFSGVGSRPGRGLEKRWGSDFDRSSTVSAPVS
PRKAHVGPREEPC--PGRKSEEPEECGSVRSGTGGRAGRGPQKRWGSDFSPASTVSAPVS
2093
RASSAT-RGSGEDRARSSLSFSLSGSPSSRRRSTSRLDSLSSAISPSWNRASGLGRESPD
RASSATRRGSGEDRAGSSLSFSLSGSPGSR-RSTSRLDSLSRTLSPSLSRASGLGRESPD
2152
SRLSLGQSCLDEWDDGASVALSEAHSQFSHPSLARSLSVPPQPRGSSSASASVIEGSSVR
SRLSLGRSCLEEWDDGASMALSEACSQYSHPSLARSLSVPPRPRSSASAVD-EPPSSSVR
2212
PVSRHSYLDPDLEAAINEVLSYKPVPFQRSRLEPDSEDDDRKSIQSARSAQLEHPERGSS
SVSRHSYLDPDLEAAVNEVLSYKPVPFQRSSLEPDSEEDDRKSIQSARSAQLDPPERAAS
2272
IRRSASAADVSS-RSGRKSRSKHRSKRSSPSPSSSSSSSSSSSSEGSSAHKRRRKGRSR
IRRSASAADVSRSRSGRKSRSRRRSGRSSS-------SSSSSSGSEASSEHKRRKKGRSR
2331
KSKKKS-KSRRKKTESESESSSSSGSTVSGHSRSSVKKGPTTDVEEAGQTPRRSKKEEKQ
KSKKSKSRRKRTETESESSSSSSSGSTVSSHSCSSVKKGPAAESEETGQTHRPSRKEEKK
2390
RKKEVDSLMMRYLYRPESD
RKKEVDSLMMRYLYRPESD
2409

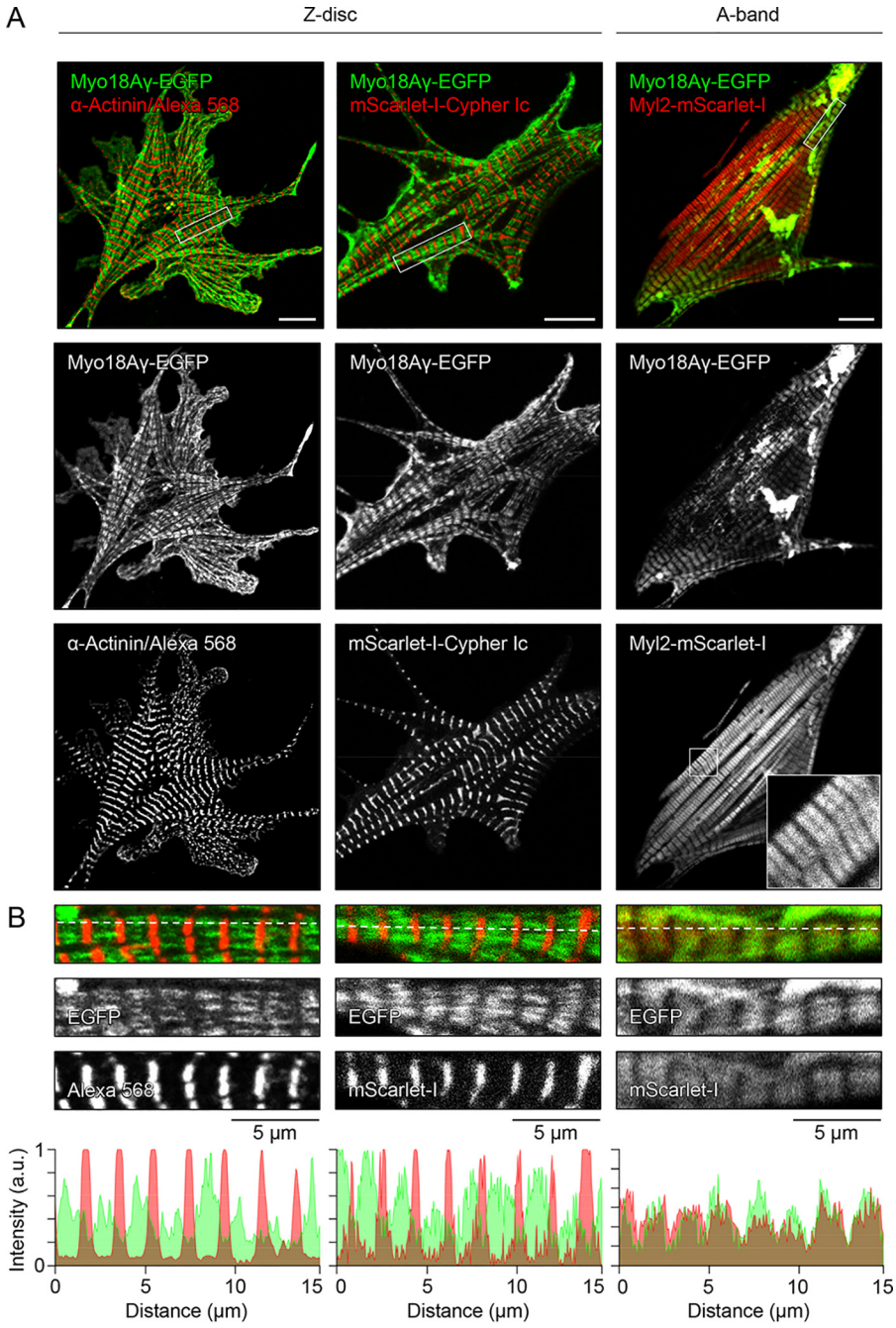


**Figure 6. Subcellular localization of Myo18A$\gamma$ in neonatal rat ventricular cardiomyocytes.** *A*, NRVMs were lipofected with expression plasmids encoding EGFP-tagged mouse Myo18A$\gamma$ (Myo18A$\gamma$-EGFP; *middle row*) and mScarlet-I-tagged mouse Cypher 1c (*middle column*) or mScarlet-I–tagged rat Myl2 (*right column*). Alternatively, cells fixed 4 days post-transfection were labeled with antibodies directed against sarcomeric $\alpha$-actinin (*left column*). Images were obtained by laser-scanning confocal microscopy. *Scale bars*, 10 $\mu$m. *B*, *enlarged views* of the rectangular regions of interest shown in the *top row* of *A*. A *horizontal line* was drawn across these regions of interest to obtain the corresponding density plots, shown below. *a.u.*, arbitrary units.

Myo18A$\beta$ protein (Fig. 9, *C* and *D*). Both Myo18A$\alpha$ and Myo18A$\beta$ (Myo18A$\alpha$ > Myo18A$\beta$) could be detected in HeLa and NIH-3T3 cells.

Next, we investigated the impact of *Myo18a* deficiency on macrophage cell shape, motility, and chemotaxis. Using real-time chemotaxis assays, we observed no significant differences

**Figure 5. Human homolog of mouse Myo18A$\gamma$ and mouse–human sequence alignment.** *A*, representative Sashimi plot of data obtained by RNA-Seq analysis of human atrial tissue ($n$ = 10 subjects). Exons are *colored blue*, and splice junction reads are depicted as *arcs*. The *red rectangles* indicate exons that are detected in the human atrial tissue transcript but absent in the aligned genomic references corresponding to transcripts (a–f) for human MYO18A. The accession numbers are as follows: MYO18Aa (NM_078471), MYO18Ab (NM_203318), MYO18Ac (NM_001346765), MYO18Ad (NM_001346766), MYO18Ae (NM_001346767), and MYO18Af (NM_001346768). *B*, sequence alignment of the N and C termini (*N-* and *C-term*) of mouse (*Mus musculus* (*Mus-mus*)) Myo18A$\gamma$ with human (*Homo sapiens* (*Hom-sap*)) atrial MYO18A. Identical residues are *highlighted* in *gray* and indicated by an *asterisk below* the alignment. Conserved mutations (residues replaced by another amino acid with similar biochemical properties) are indicated by a *colon*, and semiconserved mutations are denoted by a *period*. The *red numbers below* the sequences for *Homo sapiens* correspond to the (*red*) numbered exons depicted in the Sashimi plot *above*.

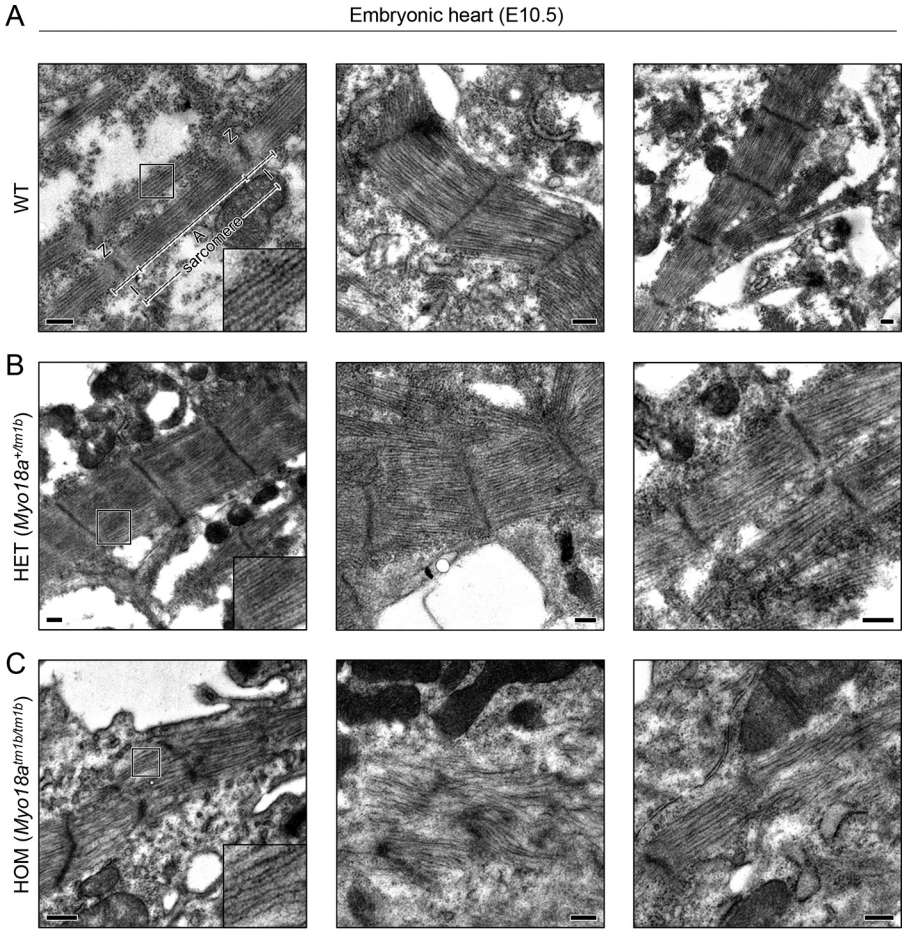


**Figure 7. Ultrastructural analysis of *Myo18a*-deficient E10.5 embryo hearts.** *A* and *B*, high-magnification images, obtained by transmission EM, showing well-defined sarcomeres in WT and HET *Myo18a* knockout (*Myo18a*$^{+/tm1b}$) E10.5 embryo hearts. The *insets* indicate parallel bundled filaments. *C*, highly disorganized sarcomeres in HOM *Myo18a* knockout (*Myo18a*$^{tm1b/tm1b}$) E10.5 embryo hearts. *Z*, Z-disc; *I*, I-band; *A*, A-band. *Scale bars*, 250 nm.

in the morphological polarization, motility, or chemotactic efficiency of WT *versus Myo18a*-deficient macrophages in a complement C5a (chemoattractant) gradient (Fig. 9, *E* and *F*). These findings were surprising because Myo18A has been implicated in the regulation of cytoskeletal dynamics and cell motility (14).

### *Golgi morphology in WT and Myo18a conditional knockout macrophages*

Myo18A has been reported to link the *trans*-Golgi to the actin cytoskeleton and provide the tension required for its characteristic morphology (9), a stack of elongated flattened cisternae (24). To image the Golgi apparatus, we used anti-GM130 (*cis*-Golgi matrix protein) and anti-Giantin (Golgi membrane protein) antibodies as markers of the *cis*-Golgi and Golgi complex, respectively. The Golgi complex was imaged by superresolution structured illumination microscopy (SR-SIM). To confirm that the system (Zeiss Elyra S.1 SIM microscope) could resolve structures beyond the diffraction limit, we measured point spread functions of subdiffraction-sized (100-nm diameter) fluorescent beads (Fig. 10*A*). The width of point spread functions at half-maximal intensity, full width at half-maximum, was used as an index of resolution (25). The median lateral resolution was $x = 108$ nm/$y = 116$ nm using the 488-nm laser and $x = 116$ nm/$y = 131$ nm using the 561-nm laser (Fig. 10*A*), whereas the axial resolution was 316 nm (488-nm laser) and 359 nm (561-nm laser), respectively (not shown). SR-SIM revealed no differences between WT and *Myo18a* conditional knockout macrophages in the geometry or location of the *cis*-Golgi or Golgi complex (Fig. 10, *B* and *C*). Furthermore, no localization of Myo18A to the Golgi complex could be observed in living HeLa cells expressing both Myo18A-EGFP and RFP-Golgi, a Golgi probe (Fig. 10*D*). Taken together, these data suggest that Myo18A is not critical for the development or maintenance of Golgi morphology.

## Discussion

We investigated the expression of the unconventional myosin Myo18A and the phenotypes of various *Myo18a* knockout mouse models, which led to the identification of a novel cardiac isoform of Myo18A (Myo18A$\gamma$) as a critical sarcomere component. More specifically, we found that (i) homozygous deletion of *Myo18a* is embryonic lethal; (ii) *Myo18a* is highly expressed in the embryo heart; (iii) a novel isoform of Myo18A (Myo18A$\gamma$) with unique N and C termini, and larger than previously known isoforms, is expressed in the heart; (iv) EGFP-tagged Myo18A$\gamma$ localizes to the sarcomere with A-band-like interruptions; (v) cardiac-restricted *Myo18a* deletion is embryonic lethal; and (vi) sarcomeres are disorganized in *Myo18a* knockout embryo hearts. In addition, we found that (vii) Myo18A$\beta$ > Myo18A$\alpha$ is expressed in mouse resident macro-

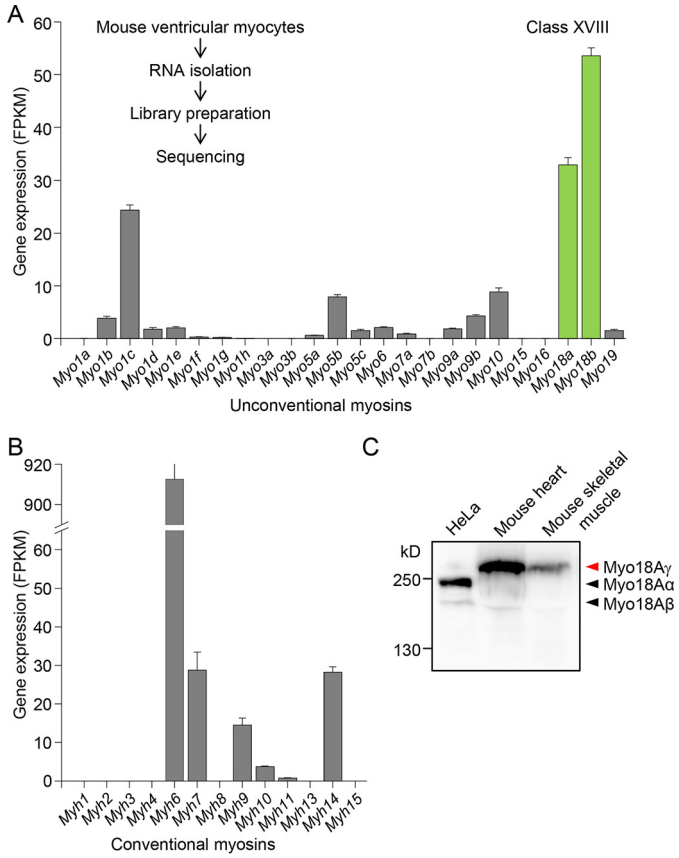


**Figure 8. *Myo18a* and *Myo18b* are the predominantly expressed unconventional myosins in mouse ventricular myocytes, and Myo18Aγ is detected in both mouse cardiac and skeletal muscle.** *A*, expression levels of unconventional myosins in mouse ventricular myocytes. Data were obtained by RNA sequence analysis ($n = 6$ mice), and expression levels are indexed as FPKM (fragments per kilobase of transcript per million mapped reads). *B*, expression levels of conventional (class II) myosins in mouse ventricular myocytes. Note that *Myh6*, the dominant cardiac-specific myosin heavy chain isoform in adult mice, is highly expressed (2 of the 6 samples exceeded the detection range; not shown). *C*, Western blot analysis. Anti-Myo18A coiled-coil domain antibodies were used to detect Myo18A isoforms expressed in HeLa cells, mouse heart, and mouse skeletal (gastrocnemius) muscle. *Error bars*, S.E.

phages, and (viii) macrophages isolated from myeloid-restricted *Myo18a* knockout mice have normal motility and Golgi morphology. Interestingly, the other class XVIII myosin, Myo18B (as distinct from Myo18Aβ), has been previously reported to be highly expressed in mouse embryo heart and to localize to the sarcomeres of striated muscle, and *Myo18b* deletion is embryonic lethal (7). Thus, our findings i–vi underscore that both class XVIII myosins (Myo18A and Myo18B) are integral components of sarcomeres, and neither member can compensate for the loss of the other. The negative findings in *Myo18a*-deficient macrophages, as well as the recent work from Bruun *et al.* (10), suggest that Myo18A may not be essential for cell motility or Golgi shape, as deduced previously from knockdown studies (9, 14, 26). Interestingly, Cao *et al.* (26) observed that knockdown of *myo18a* (*Myo18a*) in zebrafish led to distorted myofibers, which the authors attributed to loss of Golgi binding to F-actin via the PDZ domain of Myo18A. Alternatively, the distortion of myofibers could, in principle, be due to impaired sarcomere assembly and/or stability.

Surprisingly, we found that the cardiac isoform of Myo18A (Myo18Aγ) lacks an N-terminal KE-rich region and PDZ domain, a hallmark of Myo18A. Instead, the N terminus of Myo18Aγ harbors a polyproline region (PKPPPPPPPPPAP-PKP), which probably adopts a polyproline II helix (27). This region, which contains both class I ([+]-*X*-hydrophobic-P-*X*-*X*-P) and class II (P-*X*-hydrophobic-P-*X*-[+]) consensus motifs (28), may bind to SH3 (Src homology 3) domains. Class I and class II consensus motifs were also found in the N termini of Myo18Aγ homologs identified in humans (Fig. 5) and other species (Fig. S3). The alternative C terminus of Myo18Aγ is 388 amino acids longer than in Myo18Aα (see Fig. 4 and Fig. S2) and is rich in serines, exemplified by a stretch of 13 consecutive serine residues. Alignments indicated that the N and C termini of mouse Myo18Aγ are highly conserved in human heart (Fig. 5), as well as in inferred protein sequences from other mammalian species (Figs. S3 and S4). Multiple conserved blocks, segments of protein, can be identified in both the N and C termini (Fig. 5 and Figs. S3 and S4). We speculate that Myo18Aγ may form higher-order structures and serve as a molecular scaffold for sarcomere assembly and maintenance. In support of this notion, the head domain (subfraction-1) of Myo18Aγ is similar to Myo18Aα and Myo18Aβ and has been shown to lack motor activity (11–13). Future studies using antibodies specifically recognizing the novel N and C termini of Myo18Aγ, combined with superresolution imaging and EM, as well as screening for protein interaction partners, may help to resolve how Myo18Aγ regulates sarcomere assembly and function.

In conclusion, we show using knockout mouse models, gene expression analyses, and imaging that the unconventional myosin Myo18A, which lacks motor activity, is an essential sarcomeric protein. We also show that a novel isoform of Myo18A, Myo18Aγ (267 kDa), rather than the known isoforms Myo18Aα (230 kDa) and Myo18Aβ (190 kDa), is expressed in the heart, as well as in skeletal muscle. Myo18Aγ localizes to A-bands, and loss-of-function leads to disorganization of sarcomeres. Thus, both class XVIII myosins (Myo18A and Myo18B) have specialist functions in sarcomeres.

## Experimental procedures

### *Mice*

Heterozygous *Myo18a* knockout first mice (C57BL/6N-*Myo18a*$^{tm1a(KOMP)Wtsi}$) were obtained from KOMP (University of California, Davis, CA). The knockout first (preconditional) allele, designated tm1a, is a null (nonexpressive) allele because the internal ribosome entry site (*IRES*)/*lacZ* cassette contains a Simian virus 40 polyadenylation site, which terminates transcription (29). The gene trap (*IRES*/*lacZ*), as well as the *neo* selection cassettes, are flanked by *FRT* sites, whereas, additionally, both the *neo* cassette and exons 8, 9, and 10 of *Myo18a* are flanked by *loxP* sites in the *Myo18a*$^{tm1a}$ allele. We converted the knockout first allele to a conditional allele (in which gene function is restored) by crossing heterozygous *Myo18a* knockout first (*Myo18a*$^{+/tm1a}$) mice with Flp deleter mice (30). The resulting floxed *Myo18a* (C57BL/6N-*Myo18a*$^{tm1c}$) mice were crossed with PGK-Cre (*Tg*(*Pgk1-cre*)*1Lni*) mice (31), which express Cre recombinase, to produce heterozygous *Myo18a*-defi-

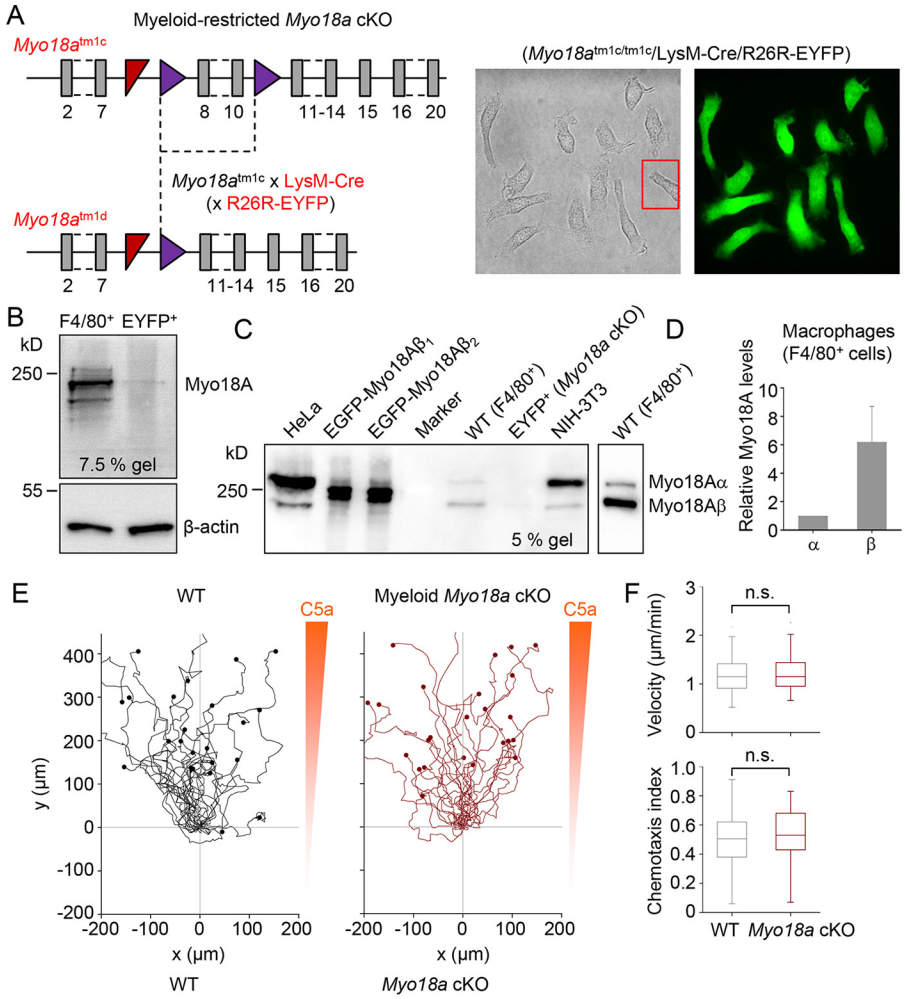


**Figure 9. Generation of myeloid-restricted *Myo18a* knockout mice and expression of the splice variants Myo18A$\alpha$ and Myo18A$\beta$ in macrophages.** *A*, triple mutant *Myo18a* cKO mice. Shown is a *schematic diagram* of the floxed *Myo18a* allele (*Myo18a*$^{tm1c}$) and conversion to a myeloid-restricted Myo18a knockout allele with a fluorescent reporter (R26R-EYFP) of Cre recombinase activity. The bright field and fluorescence images on the *right*, obtained by spinning disk confocal microscopy, show resident peritoneal macrophages isolated from a *Myo18a*$^{tm1c/tm1c}$/LysM-Cre/R26R-EYFP mouse. Images are 120 × 120 $\mu$m. *B*, Western blot analysis of purified WT (F4/80$^+$ cells) *versus* conditional *Myo18a* knockout macrophages (EYFP$^+$ cells). In each lane, lysate from 2 × 10$^5$ cells was loaded. *C*, Western blot analysis of Myo18A protein detected in the following cell lysates: untransfected (human) HeLa cells, HeLa cells transfected with mouse EGFP-Myo18A$\beta_1$, HeLa cells transfected with mouse EGFP-Myo18A$\beta_2$, 1.5 × 10$^5$ purified peritoneal F4/80$^+$ cells (macrophages) from WT mice, 1.5 × 10$^5$ purified peritoneal EYFP$^+$ (Cre recombinase–positive) cells from *Myo18a*$^{tm1c/tm1c}$/LysM-Cre/R26R-EYFP mice, and (mouse) NIH-3T3 cells. A separate blot shows the relative intensities of Myo18A alternative splicing isoforms. *D*, relative protein levels of Myo18A$\alpha$ ($\alpha$) and Myo18A$\beta$ ($\beta$) in purified mouse resident macrophages. *Error bars*, S.E. *E*, migration plots of WT and *Myo18a*-deficient macrophages in a complement C5a gradient. *F*, summary plots of chemotactic efficiency (chemotaxis index) and mean velocity ($n$ = 100 cells (4 mice) in each group); *n.s.* = not significant at the 0.05 level of significance (Mann–Whitney *U* test). Rabbit polyclonal anti-Myo18A antibody (14611-1-AP; Proteintech Europe) was used for the above Western blotting analyses.

cient (*Myo18a*$^{+/tm1d}$) mice. We also converted the knockout first allele to a knockout reporter allele (*Myo18a*$^{+/tm1b}$) by crossing heterozygous *Myo18a* knockout first mice with ACTB-Cre deleter (C57BL/6N-*Gt(ROSA)26Sor*$^{tm1(ACTB-cre,-EGFP)lcs}$) mice (32). Heterozygous knockout mice (tm1b or tm1d) were interbred to screen for embryonic lethality. Alternatively, floxed *Myo18a* mice were crossed with LysM-Cre mice (23), in which Cre recombinase expression is restricted to myeloid cells. *Myo18a*$^{tm1c/tm1c}$/LysM-Cre mice were crossed with Cre reporter (B6.129X1-*Gt(ROSA)26Sor*$^{tm1(EYFP)Cos}$/J) mice (also known as R26R-EYFP mice), which express the fluorescent protein EYFP after Cre recombination and removal of the floxed stop sequence (33). Cardiac-restricted *Myo18a* conditional knockout mice were produced by crossing *Myo18a*$^{tm1c/tm1c}$ or *Myo18a*$^{tm1c/tm1c}$/R26R-EYFP mice with *Myo18a*$^{+/tm1c}$/*Tnnt2*-Cre (Tg(*Tnnt2*-cre)5Blh/JiaoJ) mice (19). In short, we used or generated the following mice: *Myo18a*$^{+/tm1a}$ (heterozygous knockout first), *Myo18a*$^{+/tm1b}$ (heterozygous knockout reporter), *Myo18a*$^{tm1c/tm1c}$ (homozygous floxed), *Myo18a*$^{tm1c/tm1c}$/LysM-Cre (myeloid-restricted *Myo18a* knockout), *Myo18a*$^{tm1c/tm1c}$/LysM-Cre/R26R-EYFP (myeloid-restricted *Myo18a* knockout with fluorescent Cre reporter) and *Myo18a*$^{+/tm1d}$ (heterozygous knockout), *Myo18a*$^{tm1c/tm1c}$/*Tnnt2*-Cre (cardiac-restricted *Myo18a* knockout), and *Myo18a*$^{tm1c/tm1c}$/*Tnnt2*-Cre/R26R-EYFP (cardiac-restricted *Myo18a* knockout with fluorescent Cre reporter).

All animal work done at the Centre for Phenogenomics was performed in compliance with the Animals for Research Act of Ontario and the Guidelines of the Canadian Council on Animal Care. The Centre for Phenogenomics' Animal Care Committee reviewed and approved all procedures conducted on animals at the Centre for Phenogenomics. All work with animals at the

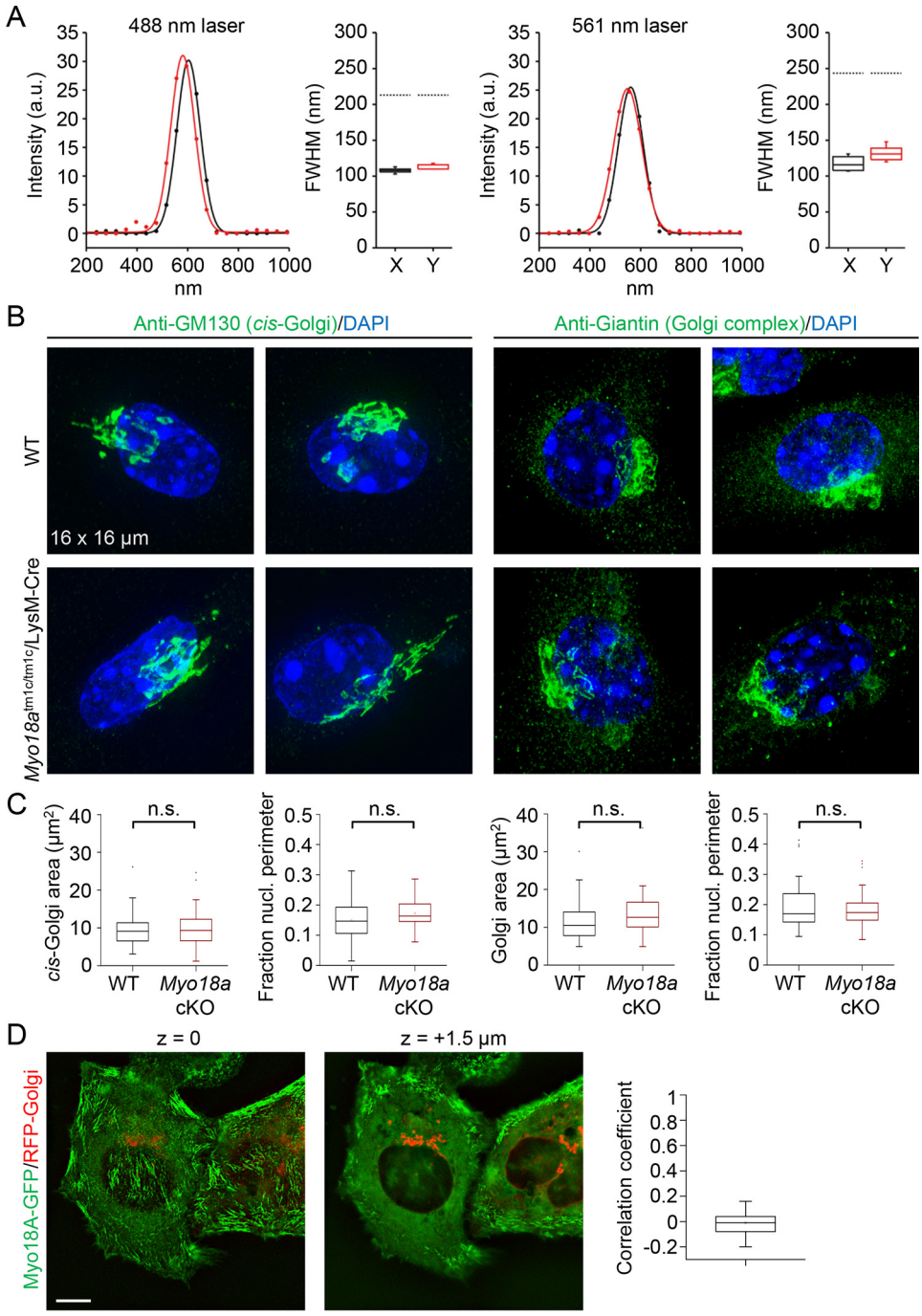


**Figure 10. Myo18A does not localize to Golgi and *Myo18a*-deficient macrophages have normal Golgi morphology.** *A*, resolution of the Zeiss Elyra superresolution structured illumination microscope (SR-SIM) determined by point spread function measurements. Subdiffraction-sized fluorescent beads (100 nm diameter) were imaged via a ×63 oil immersion objective lens (numerical aperture 1.46), and stacks were obtained at 110-nm steps. *B*, SR-SIM images of fixed WT and *Myo18a*-deficient (*Myo18a*$^{tm1c/tm1c}$/LysM-Cre; cKO) macrophages labeled with anti-GM130 (*cis*-Golgi) or anti-Giantin (Golgi membrane) antibodies (*green*) and the nucleic acid stain 4′,6-diamidino-2-phenylindole (*blue*). *C*, summary plots of Golgi area and Golgi extent (the fraction of the nuclear perimeter overlapped by Golgi cisternae) in WT *versus* *Myo18a*-deficient macrophages; *n.s.*, not significant at the 0.05 level of significance (Mann–Whitney *U* test). *D*, SR-SIM images of living HeLa cells stably transfected with Myo18A-EGFP (*green*) and transiently transfected with the Golgi probe RFP-Golgi (*red*). *Right*, box plot of Pearson's correlation coefficient. *Scale bar*, 10 $\mu$m.

University of Münster was performed in accordance with the German Animal Welfare Act (Tierschutzgesetz) and approved by the local ethics committee of the University of Münster. All animal experiments performed at the Leiden University Medical Center were approved by the animal experiments committee and conformed to the Guide for the Care and Use of Laboratory Animals of the United States National Institutes of Health.

### *Genotyping*

PCR for genotyping was performed in two phases. First, touchdown PCR was performed using the following thermocycling protocol: 94 °C for 7 min and then 10 cycles of 94 °C for 30 s, 65 to 55 °C (starting at 65 °C and subtracting 1 °C each cycle) for 30 s, and 72 °C for 60 s. This was followed by 30 cycles of 94 °C for 30 s, 55 °C for 30 s, and 72 °C for 60 s. The following

primer sequences (5′ → 3′) were used (product sizes shown in parentheses): tm1a allele 3′ (687 bp): forward (common loxP-F), GAGATGGCGCAACGCAATTAAT; reverse (*Myo18a*-R1), TGGGTGAAGAGCTGCTATAATCCTGG; WT allele (298 bp): forward (*Myo18a*-F1), AGGCACAGTGATCTCTTCACACTG; reverse (*Myo18a*-R2), CAAGTTGCCCTCTGACCTCCATG; tm1b allele (after tm1a Cre-loxP recombination) (482 bp): forward (TCP-LacF), CCATTACCAGTTGGTCTGGTGTC; reverse (*Myo18a*_tm1b_R1) ATCCCTCAACCCTACATCCAAGCCAC; tm1c (floxed) allele (after Flp-FRT recombination) (482 bp): forward, *Myo18a*-F1 (as above); reverse (*Myo18a*-R4), GCCTACTGCGACTATAGAGATATCAACC; tm1d allele (after crossing *Myo18a*$^{tm1c}$ and PKG-Cre mice) (505 bp): forward, *Myo18a*-F1 (as above); reverse (*Myo18a*-R5), TCGCTCCTCACTCTGTCTTGAAAGC; LysM-Cre allele (490 bp): forward (Cre-F), CCAATTTACTGACCGTACACC; reverse (Cre-R), TATATCCTGGCAGCGATCGC. Primer sequences (5′ → 3′) for genotyping the R26R-EYFP strain were as follows: mutant, AAGACCGCGAAGAGTTTGTC; common, AAAGTCGCTCTGAGTTGTTAT; WT, GGAGCGGGAGAAATGGATATG. The PCR product sizes (in parentheses) are as follows: homozygous mutant (320 bp), heterozygote (320 and 600 bp), and WT (600 bp). ACTB-Cre mice were genotyped by observing EGFP fluorescence in neonate pups.

### *HR1 and HR2 Southern probe cloning*

The Myo18_HR1 Southern DNA probe was cloned as follows. The 1353-bp DNA fragment corresponding to the HR1 region was PCR-amplified from 129Sv mouse genomic DNA using primers Myo18_HR1d1 and Myo18_HR1r2 and cloned using the Golden Gate cloning method (34). The 2224-bp DNA fragment (Myo18_HR2 probe) was PCR-amplified using primers Myo18_HR2d3 and Myo18_HR2r4 and cloned accordingly. The primer sequences were as follows: Myo18_HR1d1 (GTCTCAAGCGTCTCTTGGATCCCACCTGGTAGGAATGTTAG), Myo18_HR1r2 (GCTCTAGACGTCTCTGAGAATTCCAATTTTCACAGCAAGAG), *Myo18a*_HR2d3 (GTCTCAAGCGTCTCTTGGACGATCTAGAATCACGGTTGCTCT), and Myo18_HR2r4 (GCTCTAGACGTCTCTGAGATTCCCAGTACTTAAGGCGTCAC).

### *DNA Southern blot analysis*

Mouse genomic DNA, isolated from tail biopsies using the water/phenol method, was analyzed by Southern blotting DNA hybridization. Approximately 5 mg of genomic DNA was digested with EcoRI, fractionated on 0.8% agarose gels, and transferred to GeneScreen nylon membranes (NEN DuPont, Boston, MA). The membranes were hybridized with a $^{32}$P-labeled probe containing sequences 5′ or 3′ to the targeted homology (HR probes) and washed with (final concentrations) 0.5× SSPE (1× SSPE is 0.18 M NaCl, 10 mM $NaH_2PO_4$, and 1 mM EDTA, pH 7.7) and 0.5% SDS at 65 °C.

### *lacZ staining*

Whole-mount lacZ staining and gene expression analysis was performed using embryos as described by Tuck *et al.* (35) and by Adams and Gale (46), cited therein. Briefly, embryos were dissected in 1× PBS, and pieces of embryo-derived yolk sac were transferred to 96-well plates for genotyping. Embryos were dissected away from extraembryonic tissue and fixed in individual wells of a 12-well plate with 2.5 ml of fixative (1% neutral buffered formalin, 0.2% glutaraldehyde, 2 mM $MgCl_2$, 5 mM EDTA, and 0.02% IGEPAL CA-630 in 1× PBS) on a rocking platform for 30 min at room temperature. Embryos were washed three times for 10 min each in 1× PBS, pH 8.5, 0.02% IGEPAL and then stained for 18 h at room temperature or 48 h at 4 °C in the dark in 5 mM $K_3Fe(CN)_6$, 5 mM $K_4Fe(CN)_6$, 2 mM $MgCl_2$, 0.02% IGEPAL, and 1 mg/ml X-gal in 1× PBS (pH 8.5). After staining, embryos were washed two times for 10 min each in 1× PBS with 0.1% Tween 20 at room temperature in the dark followed by 18 h of post-fixation in 10% neutral buffered formalin. Embryos were then cleared with sequential incubation in 20% glycerol in 1% KOH for 8 h at 37 °C, 50% glycerol in 1% KOH for 24–72 h at 37 °C, followed by 70% glycerol in 1× PBS for at least 1 week at room temperature prior to imaging.

### *Antibodies*

Affinity-purified polyclonal (anti-mMyo18A) antibodies suitable for immunofluorescence imaging were produced in New Zealand White rabbits immunized with a synthetic peptide (HSYLSDSDTEAKLTETSA) corresponding to the last 18 amino acids of the C terminus of mouse Myo18A (a peptide antigen kindly recommended by John A. Hammer). An attempt to obtain polyclonal antibodies against a synthetic peptide (LMKKDKDKDGGRKEKK) specific for the N-terminal extension of mouse Myo18A was unsuccessful. Rabbit polyclonal anti-Myo18A antibody (14611-1-AP; Proteintech Europe, Manchester, UK), diluted 1:1000, was used to detect mouse Myo18A protein by Western blotting. Lysates from HeLa cells expressing EGFP-tagged mouse Myo18A$\alpha$ or Myo18A$\beta$ were used as positive controls for the antibody. In addition, anti-Myo18A coiled-coil domain (tail domain) antibodies were obtained from Santa Cruz Biotechnology, Inc. (amino acids (human) 1656–1780; catalogue no. sc-99127). Macrophages were purified by cell sorting using rat anti-mouse F4/80 antibodies conjugated to Alexa Fluor 488 (1:40, MCA497A488, Bio-Rad AbD Serotec). For immunofluorescence imaging of *cis*-Golgi and the Golgi complex (in fixed mouse macrophages), mouse monoclonal anti-GM130 antibodies (clone 35/GM130; 610822, BD Biosciences) and rabbit polyclonal anti-Giantin antibodies (ab24586; Abcam) were used, respectively.

### *Isolation of mouse ventricular myocytes*

Perfusion medium (200 ml) contained 113 mM NaCl, 4.7 mM KCl, 0.6 mM $KH_2PO_4$, 0.6 mM $Na_2HPO_4{\cdot}2H_2O$ (dihydrate), 1.2 mM $MgSO_4{\cdot}7H_2O$, 12 mM $NaHCO_3$, 10 mM $KHCO_3$, 30 mM taurine, 10 mM 2,3-butanedione monoxime, 2 g/liter glucose, and 10 mM Hepes (pH titrated to 7.47 by the addition of 10 M NaOH). The digestion medium (25 ml) contained collagenase type II (190 units/ml), protease type XIV (0.33 units/ml), and 12.5 $\mu$M $CaCl_2$. The adult mouse heart was perfused with perfusion medium for 5 min at a rate of ~2.5 ml/min, followed by ~6-min perfusion with digestion medium. Subsequently, the heart was placed in 2.5 ml of digestion medium, and the remnant aorta, as well as the atria, were excised. Two tweezers were used to tear apart the heart, and cells were further dissociated

by repeated aspiration and dispersion via a 10-ml plastic pipette. Perfusion medium (2.5 ml) supplemented with 10% newborn calf serum (NBCS) was added (1:1) to inhibit collagenase and protease activity. After a 10-min sedimentation time, the supernatant was discarded, and cells were resuspended with 7 ml of perfusion medium supplemented with 5% NBCS. Resuspended cells were passed through a nylon filter, and an additional 3 ml of perfusion medium containing 5% NBCS was added, yielding 10 ml of suspended ventricular myocytes.

### *RNA-Seq*

Total RNA of isolated primary ventricular myocytes and human atrial tissue was isolated using TRIzol (Thermo Fisher Scientific) and the Direct-zol RNA MiniPrep Kit (Zymo Research, Freiburg, Germany). Atrial appendages were received from patients with sinus rhythm undergoing open-heart surgery. Permission for experiments with atrial tissue was obtained from the ethics committee of the Technische Universität Dresden (reference number EK 446122011). The investigation conformed to the principles outlined in the Declaration of Helsinki.

Small RNA libraries were prepared for next-generation sequencing by Illumina sequencing using the following kits/modules from New England Biolabs: the NEBNext Poly(A) mRNA Magnetic Isolation Module (used to isolate poly(A)$^+$ RNA from total RNA), NEBNext Multiplex Oligos, and the NEBNext Ultra RNA Library Prep Kit. Quality control and quantification of the prepared libraries were performed on a 2100 Bioanalyzer (Agilent Technologies, Waldbronn, Germany). Libraries were sequenced on a HiScanSQ sequencing system (Illumina, San Diego, CA) in a single-end mode (50 bp) using a TruSeq SR Cluster version 3 and a TruSeq SBS version 3 kit (both Illumina). Validated sequences were mapped, and the Integrative Genomics Viewer (36) was used to visualize splice junctions of the *Myo18a* gene in a Sashimi plot.

### *Plasmids for transfection of rat neonatal cardiomyocytes*

Expression plasmids were constructed using standard molecular cloning techniques. Restriction and DNA-modifying enzymes (Fermentas, Thermo Fisher Scientific (Breda, The Netherlands) or New England Biolabs, Bioké (Leiden, The Netherlands)) and oligodeoxyribonucleotides (Sigma-Aldrich) were used, following the manufacturer's instructions. For live sarcomeric Z-line imaging, we constructed an expression plasmid named pLV.HsUBC.mScarlet-I~MmCypher1c, in which the coding sequence of the murine Cypher 1c protein (37) was preceded by a human ubiquitin C gene promoter (38) and extended at the N terminus with the coding sequence of mScarlet-I (39) (AddGene plasmid number 85044). For live-cell imaging of the sarcomeric A-band, the expression plasmid pLV.HsUBC.RnMyl2~mScarlet.WHVoPRE was made. In this construct, the coding sequence of rat regulatory myosin light chain 2 is C-terminally extended with the coding sequence of mScarlet-I. Expression of the resulting fusion protein is under the control of the human ubiquitin C gene promoter.

To determine the subcellular location of Myo18A$\gamma$, the expression plasmid pEGFP-N1-Myo18A$\gamma$ was generated. In this construct, the coding sequence of mouse Myo18A$\gamma$ protein was extended at its C terminus with the coding sequence of enhanced GFP. Expression of the resulting fusion protein is controlled by the human cytomegalovirus immediate-early gene promoter.

### *Isolation and culture of rat neonatal cardiomyocytes*

Ventricular cardiomyocytes were isolated from the hearts of neonatal Wistar rats and cultured as described previously (40). Briefly, 2-day-old neonatal Wistar rats were anesthetized using 5% isoflurane inhalation. After adequate anesthesia was confirmed, the hearts were rapidly excised, atria and ventricles were separated, and the ventricular tissue was finely minced and dissociated by two subsequent treatments of 30 min with collagenase type I (Worthington) and DNase I (Sigma-Aldrich). Cells were pelleted by centrifugation (10 min, room temperature, 160 $\times$ *g*) and resuspended in growth medium. The cell suspension was transferred to Primaria$^{TM}$ culture dishes (Corning Life Sciences, Amsterdam, The Netherlands) and incubated for 75 min at 37 °C in a humidified atmosphere of 95% air and 5% $CO_2$. The unattached cells, predominantly NRVMs, were collected and passed through a 70-$\mu$m cell strainer (BD Biosciences). Subsequently, $5 \times 10^4$ NRVMs were seeded in 500 $\mu$l of growth medium on fibronectin-coated (Sigma-Aldrich) coverslips in a 24-well culture plate (Corning Life Sciences). To prevent the proliferation of noncardiomyocytes, ~20 h after seeding, the cultures were treated for 2 h with growth medium containing mitomycin-C (10 $\mu$g/ml; Sigma-Aldrich, catalogue no. M4287) (41). After this treatment, the growth medium was replaced by culture medium.

Growth medium consisted of Ham's F10 medium (Thermo Fisher Scientific, catalogue no. 11550) supplemented with 100 units/ml penicillin, 100 $\mu$g/ml streptomycin, 5% fetal bovine serum, and 10% heat-inactivated horse serum. Culture medium contained a 1:1 mixture of low-glucose DMEM (Thermo Fisher Scientific, catalogue no. 22320) and Ham's F10 medium (Thermo Fisher Scientific, catalogue no. 11550) supplemented with BSA (0.2%; Sigma-Aldrich, catalogue no. A6003), sodium L-ascorbate (0.1 mM; Sigma-Aldrich, catalogue no. A7631), sodium pyruvate (3.8 mM; Sigma-Aldrich, catalogue no. P2256), D-(+)-glucose (17.6 mM; Merck, catalogue no. 108337), sodium bicarbonate (0.06%; Thermo Fisher Scientific, catalogue no. 25090094), L-glutamine (0.12 mM; Thermo Fisher Scientific, catalogue no. 25030024), heat-inactivated horse serum (5%), penicillin (100 units/ml), and streptomycin (100 $\mu$g/ml).

### *Transfection and imaging of neonatal rat ventricular myocytes*

NRVMs were lipofected immediately after seeding. In brief, cells in the wells of a 24-well culture dish were transfected with 50 $\mu$l of lipoplexes consisting of 1.5 $\mu$l of Lipofectamine 3000, 1 $\mu$l of P3000 reagent (both from Thermo Fisher Scientific), and a total amount of 500 ng of plasmid DNA diluted in Opti-MEM I reduced serum medium (Thermo Fisher Scientific, catalogue no. 31985070). For co-transfection experiments, 250 ng of each expression plasmid was used. After 20 h, the transfection medium was replaced with growth medium containing mitomycin-C, which, after 2 h, was replaced with culture medium as described above.

Immunocytology of the NRVMs was performed as described previously (42). In short, 4 days after seeding, the cells were washed with PBS, fixed by incubation for 30 min in buffered 4% formaldehyde at 4 °C (Added Pharma, Oss, The Netherlands), washed with PBS, and permeabilized by incubation for 5 min at room temperature with 0.1% Triton X-100 (Sigma-Aldrich) in PBS. Afterward, the cells were washed with PBS and incubated for 2 h at room temperature with PBS containing normal donkey serum (0.1%; Sigma-Aldrich) and the following primary antibodies: mouse anti-$\alpha$-actinin (Sigma-Aldrich, catalogue no. A7811, dilution 1:200) and rabbit anti-cardiac troponin T (Abcam (Cambridge, UK), catalogue no. ab45932, dilution 1:200). After three washes with PBS, the coverslips were incubated at room temperature for 45 min with appropriate 200-fold diluted secondary antibodies (*i.e.* Alexa Fluor 568–conjugated donkey anti-mouse IgG (H+L), Alexa Fluor 568–conjugated donkey anti-rabbit IgG (H+L), Alexa Fluor 488–conjugated donkey anti-mouse IgG (H+L), and Alexa Fluor 488–conjugated donkey anti-rabbit 488 IgG (H+L) (Thermo Fisher Scientific, catalogue nos. A10037, A10042, A21202, and A21206, respectively). Cells were washed with PBS, the nuclei were counterstained for 10 min with Hoechst 33342 (final concentration 10 $\mu$g/$\mu$l; Thermo Fisher Scientific), and cells were washed again with PBS. Cells were imaged via a ×63/1.4 oil objective lens using a Leica TCS SP5 confocal laser scanning microscope and analyzed using Leica Application Suite X software (Leica Microsystems, Rijswijk, The Netherlands).

### *Transmission EM*

Ultrastructural analysis was performed on mouse embryonic heart samples (E10.5). Briefly, full-size embryos were fixed in PBS supplemented with 4% paraformaldehyde, 1% glutaraldehyde, and 15% picric acid, pH 7.4, at 4 °C overnight. Embryos were rinsed twice in PBS and treated with 0.5% $OsO_4$ for 45 min following several washing steps in 100 mM phosphate buffer. Samples were counterstained with uranyl acetate, dehydrated via ethanol series, and embedded in Durcupan ACM epoxy resin (Sigma-Aldrich). Ultrathin sections of the embryonic heart were prepared from resin blocks using a Leica Ultracut S ultramicrotome (Mannheim, Germany) and adsorbed to glow-discharged formvar-carbon–coated copper single-slot grids. Electron micrographs were recorded using a Zeiss LEO 906 electron microscope; images were taken with a TRS Sharpeye CCD camera (Troendle, Moorenweis, Germany).

### *Isolation of resident peritoneal macrophages*

Mice were killed by an overdose of isoflurane in air, and the peritoneal cavity was lavaged via a 24-gauge plastic catheter (B. Braun, Melsungen, Germany) using 2 × 4.5-ml ice-cold Hank's balanced salt solution without $Ca^{2+}$ or $Mg^{2+}$ (PAA, Pashing, Austria). After centrifugation (300 × *g* for 6.5 min), cells were resuspended in bicarbonate-free RPMI 1640 medium containing 20 mM Hepes (Biochrom AG, Berlin, Germany) and supplemented with 10% heat-inactivated fetal calf serum (FCS), 100 units/ml penicillin, and 100 $\mu$g/ml streptomycin (pH 7.4). The cells were seeded into fibronectin-coated $\mu$-slide I chambers or $\mu$-slide chemotaxis chambers (Ibidi, Martinsried, Germany) and placed in a humidified incubator (37 °C). After 2 h, $\mu$-slide I chambers were filled with 1 ml of RPMI 1640 medium, including 10% FCS and antibiotics, and incubated overnight at 37 °C with 5% $CO_2$. Experiments were performed on the stage of an inverted microscope (LSM 510, Zeiss) equipped with a temperature-controlled incubator (incubator XL S, Zeiss) using the same bicarbonate-free RPMI 1640 medium as above.

### *2D chemotaxis assays*

2D chemotaxis assays have been described previously (43, 44). In brief, cells obtained by peritoneal lavage of a single mouse were resuspended in 125–175 $\mu$l of medium, and 10 $\mu$l of the suspension was seeded into the narrow (1000 × 2000 × 70 $\mu$m) channel of an uncoated (IbiTreat) $\mu$-slide chemotaxis chamber (Ibidi). The narrow channel (observation area) connects two 45-$\mu$l reservoirs. After 3 h, the chemotaxis chamber was filled with bicarbonate-free RPMI 1640 medium containing 10% FCS, 100 ng/ml lipopolysaccharide, and antibiotics. Next, 15 $\mu$l of medium containing chemoattractant (complement C5a) and 0.003% Patent Blue V (blue dye) was drawn into one of the reservoirs. The final concentration of complement C5a was 20 nM. The observation area was imaged by phase-contrast microscopy via a ×10/0.3 objective lens. The blue dye served as a visual indicator of gradient formation, and we have previously confirmed that it does not affect cell migration. Images were captured every 2 min for 14 h, and cell migration tracks between 6 and 12 h were analyzed with ImageJ (National Institutes of Health) using a manual tracking plugin and the chemotaxis and migration tool from Ibidi. Twenty-five randomly selected cells were manually tracked in each chemotaxis experiment.

### *Flow cytometry and cell sorting*

Cell sorting of $EYFP^+$ cells or macrophages stained with Alexa Fluor 488–conjugated anti-F4/80 antibodies and cell analyses were performed using a BD FACSAria II (or FACSAria III) cell sorter (BD Biosciences).

### *Western blot analysis*

Cells were lysed in buffer containing 100 mM NaCl, 2 mM $MgCl_2$, 1 mM DTT, 1% Nonidet P-40, 10% glycerol, 5 mM NaF, and 1 mM $Na_3VO_4$ (sodium orthovanadate); the protease inhibitors leupeptin, aprotinin, and pefabloc (each at 10 $\mu$g/ml); and 50 mM Tris-HCl (pH 7.4). Proteins were separated by 15% SDS-PAGE and transferred onto polyvinylidene difluoride membranes (Roche Applied Sciences). Membranes were blocked for 1 h at room temperature in TBS containing 5% BSA and 0.1% Tween 20 followed by overnight incubation (4 °C) with primary antibodies. For detection, horseradish peroxidase–conjugated secondary antibodies (Dianova, Hamburg, Germany) were used in combination with SuperSignal West Pico chemiluminescence substrate (Perbio, Bonn, Germany).

### *Plasmids and stably transfected HeLa cells*

pRFP-Golgi, which labels medial- and trans-Golgi, and Lifeact-mRFPruby were provided by Theresia Stradal. In addition, the following plasmids were constructed for this study: pCMV-(m)Myo18a$\alpha$-EGFP, pCMV-(m)Myo18a$\beta_1$-mCherry, pCMV-

EGFP-(m)Myo18a$\alpha$, pCMV-EGFP-(m)Myo18a$\beta_1$, pCMV-EGFP-(m)Myo18a$\beta_2$, and pCMV-(m)Myo18a-Nter-EGFP.

### *Superresolution structured illumination microscopy*

Superresolution structured illumination microscopy was performed using an Elyra S.1 inverted microscope system (Carl Zeiss MicroImaging), controlled by ZEN 2011 SP2 software (black edition; Zeiss). Cells were imaged via a Plan Apo ×63/1.4 oil objective lens, and images were captured with an Andor iXon EM-CCD. The following lasers and filters (in parentheses) were used: 405 nm (BP 420–480 + LP 750), 488 nm (BP 495–550 nm + LP 750 nm), 561 nm (BP 570–620 + LP 750 nm), and 642 nm (LP 655 nm). Five grating positions and five phase shifts were used for each *z*-slice. Point spread functions were measured using TetraSpeck 100-nm fluorescent beads mounted on a slide (T14792; Thermo Fisher Scientific) and the protocol described by Cole *et al.* (25). Data were analyzed using the MetroloJ plug-in in the open-source platform Fiji (45).

### *Statistics*

Normality and homoscedasticity were tested using the Shapiro–Wilk and Levene tests, respectively. A one-way analysis of variance was used to test for statistical differences at the 0.05 level of significance. When the assumed conditions of normality and homogeneity of variance were not fulfilled, as in most cases, we used the nonparametric Mann–Whitney *U* test or Kruskal–Wallis one-way analysis of variance on ranks (at the 0.05 level of significance). Post hoc multiple comparisons were made using Dunn's method. Statistical analyses were performed using SigmaPlot (version 12) software (Systat Software, Erkrath, Germany) or Origin 2015 SR2 (OriginLab), and data are presented as box plots or mean ± S.E.

*Author contributions*—M. H., L. M. J. N., A. C. B., B. V. S., U. H., T. Z., S. B., F. U. M., U. R., W. A. L., A. A. F. d. V., M. B., and P. J. H. designed experiments. M. H., L. M. J. N., A. C. B., B. V. S., U. H., M. S., A. U., P. R. R. v. G., M. D. S., and P. J. H. performed research and analyzed data. P. J. H. wrote the paper, with contributions from A. U., P. R. R. v. G., and A. A. F. d. V.

*Acknowledgments—We thank Amie Creighton, Patricia Castellanos Penton, and Ozge Danisment for animal husbandry, embryo dissections, lacZ staining, and embryo imaging. We also thank Ju Chen (University of California San Diego, La Jolla, CA) for providing plasmid peGFP.C1-Cypher1 encoding the murine Cypher 1c protein; Mitsuru Nenoi for donating plasmids pUbCR#1 and pUbCR#2 encoding the human ubiquitin C promoter; Iolanda Feola (Leiden University Medical Center) for NRVM isolation; and Cindy Bart, Sven Dekker, and Margreet de Jong (all from the Leiden University Medical Center) for plasmid construction.*

## References

1. Maravillas-Montero, J. L., and Santos-Argumedo, L. (2012) The myosin family: unconventional roles of actin-dependent molecular motors in immune cells. *J. Leukocyte Biol.* **91,** 35–46 CrossRef Medline
2. Hartman, M. A., Finan, D., Sivaramakrishnan, S., and Spudich, J. A. (2011) Principles of unconventional myosin function and targeting. *Annu. Rev. Cell Dev. Biol.* **27,** 133–155 CrossRef Medline
3. Furusawa, T., Ikawa, S., Yanai, N., and Obinata, M. (2000) Isolation of a novel PDZ-containing myosin from hematopoietic supportive bone marrow stromal cell lines. *Biochem. Biophys. Res. Commun.* **270,** 67–75 CrossRef Medline
4. Mori, K., Furusawa, T., Okubo, T., Inoue, T., Ikawa, S., Yanai, N., Mori, K. J., and Obinata, M. (2003) Genome structure and differential expression of two isoforms of a novel PDZ-containing myosin (MysPDZ) (Myo18A). *J. Biochem.* **133,** 405–413 CrossRef Medline
5. Mori, K., Matsuda, K., Furusawa, T., Kawata, M., Inoue, T., and Obinata, M. (2005) Subcellular localization and dynamics of MysPDZ (Myo18A) in live mammalian cells. *Biochem. Biophys. Res. Commun.* **326,** 491–498 CrossRef Medline
6. Nishioka, M., Kohno, T., Tani, M., Yanaihara, N., Tomizawa, Y., Otsuka, A., Sasaki, S., Kobayashi, K., Niki, T., Maeshima, A., Sekido, Y., Minna, J. D., Sone, S., and Yokota, J. (2002) MYO18B, a candidate tumor suppressor gene at chromosome 22q12.1, deleted, mutated, and methylated in human lung cancer. *Proc. Natl. Acad. Sci. U.S.A.* **99,** 12269–12274 CrossRef Medline
7. Ajima, R., Akazawa, H., Kodama, M., Takeshita, F., Otsuka, A., Kohno, T., Komuro, I., Ochiya, T., and Yokota, J. (2008) Deficiency of Myo18B in mice results in embryonic lethality with cardiac myofibrillar aberrations. *Genes Cells* **13,** 987–999 CrossRef Medline
8. Berger, J., Berger, S., Li, M., and Currie, P. D. (2017) Myo18b is essential for sarcomere assembly in fast skeletal muscle. *Hum. Mol. Genet.* **26,** 1146–1156 CrossRef Medline
9. Dippold, H. C., Ng, M. M., Farber-Katz, S. E., Lee, S. K., Kerr, M. L., Peterman, M. C., Sim, R., Wiharto, P. A., Galbraith, K. A., Madhavarapu, S., Fuchs, G. J., Meerloo, T., Farquhar, M. G., Zhou, H., and Field, S. J. (2009) GOLPH3 bridges phosphatidylinositol-4-phosphate and actomyosin to stretch and shape the Golgi to promote budding. *Cell* **139,** 337–351 CrossRef Medline
10. Bruun, K., Beach, J. R., Heissler, S. M., Remmert, K., Sellers, J. R., and Hammer, J. A. (2017) Re-evaluating the roles of myosin 18A$\alpha$ and F-actin in determining Golgi morphology. *Cytoskeleton* **74,** 205–218 CrossRef Medline
11. Guzik-Lendrum, S., Nagy, A., Takagi, Y., Houdusse, A., and Sellers, J. R. (2011) *Drosophila melanogaster* myosin-18 represents a highly divergent motor with actin tethering properties. *J. Biol. Chem.* **286,** 21755–21766 CrossRef Medline
12. Guzik-Lendrum, S., Heissler, S. M., Billington, N., Takagi, Y., Yang, Y., Knight, P. J., Homsher, E., and Sellers, J. R. (2013) Mammalian myosin-18A, a highly divergent myosin. *J. Biol. Chem.* **288,** 9532–9548 CrossRef Medline
13. Taft, M. H., Behrmann, E., Munske-Weidemann, L. C., Thiel, C., Raunser, S., and Manstein, D. J. (2013) Functional characterization of human myosin-18A and its interaction with F-actin and GOLPH3. *J. Biol. Chem.* **288,** 30029–30041 CrossRef Medline
14. Tan, I., Yong, J., Dong, J. M., Lim, L., and Leung, T. (2008) A tripartite complex containing MRCK modulates lamellar actomyosin retrograde flow. *Cell* **135,** 123–136 CrossRef Medline
15. Yang, C. H., Szeliga, J., Jordan, J., Faske, S., Sever-Chroneos, Z., Dorsett, B., Christian, R. E., Settlage, R. E., Shabanowitz, J., Hunt, D. F., Whitsett, J. A., and Chroneos, Z. C. (2005) Identification of the surfactant protein A receptor 210 as the unconventional myosin 18A. *J. Biol. Chem.* **280,** 34447–34457 CrossRef Medline
16. Billington, N., Beach, J. R., Heissler, S. M., Remmert, K., Guzik-Lendrum, S., Nagy, A., Takagi, Y., Shao, L., Li, D., Yang, Y., Zhang, Y., Barzik, M., Betzig, E., Hammer, J. A., 3rd, Sellers, J. R. (2015) Myosin 18A coassembles with nonmuscle myosin 2 to form mixed bipolar filaments. *Curr. Biol.* **25,** 942–948 CrossRef Medline
17. Desgrange, A., Le Garrec, J. F., and Meilhac, S. M. (2018) Left-right asymmetry in heart development and disease: forming the right loop. *Development* **145,** dev162776 CrossRef Medline
18. Perez-Garcia, V., Fineberg, E., Wilson, R., Murray, A., Mazzeo, C. I., Tudor, C., Sienerth, A., White, J. K., Tuck, E., Ryder, E. J., Gleeson, D., Siragher, E., Wardle-Jones, H., Staudt, N., Wali, N., *et al.* (2018) Placentation defects are highly prevalent in embryonic lethal mouse mutants. *Nature* **555,** 463–468 CrossRef Medline

19. Jiao, K., Kulessa, H., Tompkins, K., Zhou, Y., Batts, L., Baldwin, H. S., and Hogan, B. L. (2003) An essential role of Bmp4 in the atrioventricular septation of the mouse heart. *Genes Dev.* **17,** 2362–2367 CrossRef Medline
20. Katz, Y., Wang, E. T., Silterra, J., Schwartz, S., Wong, B., Thorvaldsdóttir, H., Robinson, J. T., Mesirov, J. P., Airoldi, E. M., and Burge, C. B. (2015) Quantitative visualization of alternative exon expression from RNA-seq data. *Bioinformatics* **31,** 2400–2402 CrossRef Medline
21. Sievers, F., and Higgins, D. G. (2018) Clustal Omega for making accurate alignments of many protein sequences. *Protein Sci.* **27,** 135–145 CrossRef Medline
22. Sievers, F., Wilm, A., Dineen, D., Gibson, T. J., Karplus, K., Li, W., Lopez, R., McWilliam, H., Remmert, M., Söding, J., Thompson, J. D., and Higgins, D. G. (2011) Fast, scalable generation of high-quality protein multiple sequence alignments using Clustal Omega. *Mol. Syst. Biol.* **7,** 539 CrossRef Medline
23. Clausen, B. E., Burkhardt, C., Reith, W., Renkawitz, R., and Förster, I. (1999) Conditional gene targeting in macrophages and granulocytes using LysMcre mice. *Transgenic Res.* **8,** 265–277 CrossRef Medline
24. Lee, I., Tiwari, N., Dunlop, M. H., Graham, M., Liu, X., and Rothman, J. E. (2014) Membrane adhesion dictates Golgi stacking and cisternal morphology. *Proc. Natl. Acad. Sci. U.S.A.* **111,** 1849–1854 CrossRef Medline
25. Cole, R. W., Jinadasa, T., and Brown, C. M. (2011) Measuring and interpreting point spread functions to determine confocal microscope resolution and ensure quality control. *Nat. Protoc.* **6,** 1929–1941 CrossRef Medline
26. Cao, J. M., Cheng, X. N., Li, S. Q., Heller, S., Xu, Z. G., and Shi, D. L. (2016) Identification of novel MYO18A interaction partners required for myoblast adhesion and muscle integrity. *Sci. Rep.* **6,** 36768 CrossRef Medline
27. Williamson, M. P. (1994) The structure and function of proline-rich regions in proteins. *Biochem. J.* **297,** 249–260 CrossRef Medline
28. Feng, S., Kasahara, C., Rickles, R. J., and Schreiber, S. L. (1995) Specific interactions outside the proline-rich core of two classes of Src homology 3 ligands. *Proc. Natl. Acad. Sci. U.S.A.* **92,** 12408–12415 CrossRef Medline
29. Skarnes, W. C., Rosen, B., West, A. P., Koutsourakis, M., Bushell, W., Iyer, V., Mujica, A. O., Thomas, M., Harrow, J., Cox, T., Jackson, D., Severin, J., Biggs, P., Fu, J., Nefedov, M., *et al.* (2011) A conditional knockout resource for the genome-wide study of mouse gene function. *Nature* **474,** 337–342 CrossRef Medline
30. Farley, F. W., Soriano, P., Steffen, L. S., and Dymecki, S. M. (2000) Widespread recombinase expression using FLPeR (flipper) mice. *Genesis* **28,** 106–110 CrossRef Medline
31. Lallemand, Y., Luria, V., Haffner-Krausz, R., and Lonai, P. (1998) Maternally expressed PGK-Cre transgene as a tool for early and uniform activation of the Cre site-specific recombinase. *Transgenic Res.* **7,** 105–112 CrossRef Medline
32. Birling, M. C., Dierich, A., Jacquot, S., Hérault, Y., and Pavlovic, G. (2012) Highly-efficient, fluorescent, locus directed cre and FlpO deleter mice on a pure C57BL/6N genetic background. *Genesis* **50,** 482–489 CrossRef Medline
33. Srinivas, S., Watanabe, T., Lin, C. S., William, C. M., Tanabe, Y., Jessell, T. M., and Costantini, F. (2001) Cre reporter strains produced by targeted insertion of EYFP and ECFP into the ROSA26 locus. *BMC Dev. Biol.* **1,** 4 CrossRef Medline
34. Engler, C., Kandzia, R., and Marillonnet, S. (2008) A one pot, one step, precision cloning method with high throughput capability. *PLoS One* **3,** e3647 CrossRef Medline
35. Tuck, E., Estabel, J., Oellrich, A., Maguire, A. K., Adissu, H. A., Souter, L., Siragher, E., Lillistone, C., Green, A. L., Wardle-Jones, H., Carragher, D. M., Karp, N. A., Smedley, D., Adams, N. C., Sanger Institute Mouse Genetics Project, *et al.* (2015) A gene expression resource generated by genome-wide lacZ profiling in the mouse. *Dis. Model. Mech.* **8,** 1467–1478 CrossRef Medline
36. Robinson, J. T., Thorvaldsdóttir, H., Winckler, W., Guttman, M., Lander, E. S., Getz, G., and Mesirov, J. P. (2011) Integrative genomics viewer. *Nat. Biotechnol.* **29,** 24–26 CrossRef Medline
37. Zhou, Q., Chu, P. H., Huang, C., Cheng, C. F., Martone, M. E., Knoll, G., Shelton, G. D., Evans, S., and Chen, J. (2001) Ablation of Cypher, a PDZ-LIM domain Z-line protein, causes a severe form of congenital myopathy. *J. Cell Biol.* **155,** 605–612 CrossRef Medline
38. Nenoi, M., Mita, K., Ichimura, S., Cartwright, I. L., Takahashi, E., Yamauchi, M., and Tsuji, H. (1996) Heterogeneous structure of the polyubiquitin gene UbC of HeLa S3 cells. *Gene* **175,** 179–185 CrossRef Medline
39. Bindels, D. S., Haarbosch, L., van Weeren, L., Postma, M., Wiese, K. E., Mastop, M., Aumonier, S., Gotthard, G., Royant, A., Hink, M. A., and Gadella, T. W., Jr. (2017) mScarlet: a bright monomeric red fluorescent protein for cellular imaging. *Nat. Methods* **14,** 53–56 CrossRef Medline
40. Engels, M. C., Askar, S. F., Jangsangthong, W., Bingen, B. O., Feola, I., Liu, J., Majumder, R., Versteegh, M. I., Braun, J., Klautz, R. J., Ypey, D. L., De Vries, A. A., and Pijnappels, D. A. (2015) Forced fusion of human ventricular scar cells with cardiomyocytes suppresses arrhythmogenicity in a co-culture model. *Cardiovasc. Res.* **107,** 601–612 CrossRef Medline
41. Askar, S. F., Ramkisoensing, A. A., Schalij, M. J., Bingen, B. O., Swildens, J., van der Laarse, A., Atsma, D. E., de Vries, A. A., Ypey, D. L., and Pijnappels, D. A. (2011) Antiproliferative treatment of myofibroblasts prevents arrhythmias in vitro by limiting myofibroblast-induced depolarization. *Cardiovasc. Res.* **90,** 295–304 CrossRef Medline
42. Yu, Z., Liu, J., van Veldhoven, J. P., IJzerman, A. P., Schalij, M. J., Pijnappels, D. A., Heitman, L. H., and de Vries, A. A. (2016) Allosteric modulation of Kv11.1 (hERG) channels protects against drug-induced ventricular arrhythmias. *Circulation Arrhythm. Electrophysiol.* **9,** e003439 CrossRef Medline
43. Kronlage, M., Song, J., Sorokin, L., Isfort, K., Schwerdtle, T., Leipziger, J., Robaye, B., Conley, P. B., Kim, H. C., Sargin, S., Schön, P., Schwab, A., and Hanley, P. J. (2010) Autocrine purinergic receptor signaling is essential for macrophage chemotaxis. *Sci. Signal.* **3,** ra55 Medline
44. Isfort, K., Ebert, F., Bornhorst, J., Sargin, S., Kardakaris, R., Pasparakis, M., Bähler, M., Schwerdtle, T., Schwab, A., and Hanley, P. J. (2011) Real-time imaging reveals that P2Y2 and P2Y12 receptor agonists are not chemoattractants and macrophage chemotaxis to complement C5a is phosphatidylinositol 3-kinase (PI3K)- and p38 mitogen-activated protein kinase (MAPK)-independent. *J. Biol. Chem.* **286,** 44776–44787 CrossRef Medline
45. Schindelin, J., Arganda-Carreras, I., Frise, E., Kaynig, V., Longair, M., Pietzsch, T., Preibisch, S., Rueden, C., Saalfeld, S., Schmid, B., Tinevez, J. Y., White, D. J., Hartenstein, V., Eliceiri, K., Tomancak, P., and Cardona, A. (2012) Fiji: an open-source platform for biological-image analysis. *Nat. Methods* **9,** 676–682 CrossRef Medline
46. Adams, N. C., and Gale, N. W. (2006) High resolution gene expression analysis in mice using genetically inserted reporter genes. In *Principle and Practice Mammalian and Avian Transgenesis: New Approaches* (Pease, S., and Lois, C., eds) pp. 132–172, Springer, New York